SPS/Note 82-40

EUROPEAN ORGANIZATION FOR NUCLEAR RESEARCH
CERN - SPS DIVISION

THE CEDAR COUNTERS FOR PARTICLE IDENTIFICATION IN THE SPS SECONDARY BEAMS : A DESCRIPTION AND AN OPERATION MANUAL

C. Bovet, R. Maleyran, L. Piemontese,
A. Placci, M. Placidi

Prévessin, 23th September 1982.

ABSTRACT

After a brief introduction on the physics of the Cerenkov effect in view of its application to particle identification, the CEDAR detectors are described, with emphasis on those characteristics and construction features which are of interest to the user. The layout of CEDAR counters in SPS secondary beams is described, and the signals provided to the user are listed and explained together with the programs for on-line control of the counter.

Finally the performances are stated, together with various hints and suggestions on the procedure to follow in order to set tune and operate a CEDAR. The dependence of CEDAR performances on beam optics is stressed.

C O N T E N T S

1. INTRODUCTION

The CERN SPS secondary beams have been instrumented with a set of various detectors, including analog wire chambers for measurement of beam spot position and size, scintillator filament scanners to optimize the beam divergence, MWPC for measurements of momentum of individual particles, and Cerenkov counters for particle identification.

The latter include threshold Cerenkov counters for applications at the lower energies, and differential counters of the DISC type for better resolution mainly at higher energies. These differential counters, called CEDAR's (Cerenkov Differential counter with achromatic ring focus) have been designed and built in the SPS Division as an experimental facility : 13 CEDARs are now operational and have been successfully operated in the North or West Area beams.

Two versions of CEDARs exist, called CEDAR-N (type) and CEDAR-W, with obvious reference to the North and West experimental areas. They differ in the energy range to which they are adapted: the CEDARs-N can separate k's from π's up to 300 GeV/c, but can detect protons only down to about 60 GeV/c, while a CEDAR-W can flag protons of 12 GeV/c, and can separate k's from π's up to about 150 GeV/c. The CEDAR's electronics is also provided and serviced by the SPS EA Group. The CEDAR commands and the electronics are under computer control, and are connected to the SPS computer network. The user receives the CEDAR signals and can operate his CEDAR from a key board in time sharing as well as he can tune his magnets and collimators.

Despite of all the facilities available it is a delicate enterprise to tune and optimize a CEDAR and to keep it in best condition during data taking. Users have to learn how to set it properly, how to check it and how to find the reason of a malfunctioning.

In chapter 2 we are describing the principles of operation and the optical resolution in order to educate the reader with the fundamental limitation of the instrument. Chapter 3 gives and comments upon all relevant parameters of the counters. Chapter 4 explains the environment of the CEDARs in a beam line, the electronic treatment of the signals and gives a thorough description of the software available for interactive controls and diagnostics. Finally in chapter 5 rules for practical operation are examplified and a complete procedure for tuning and setting-up a CEDAR is presented.

The main scope of the present report is to help the user to better understand the instrument in view of assessing its possible performances, of finding the optimum tuning for efficiency and rejection, of running and monitoring the CEDAR during all data taking.

2. PRINCIPLE OF OPERATION AND OPTICAL RESOLUTION

2.1 Principle of operation

The Cerenkov light produced by a beam particle is emitted on cones of semi-aperture θ with

$$\cos\theta = \frac{1}{n\beta} , \tag{1}$$

where n is the index of refraction of the transparent medium and β is the velocity of the particle.

Differential counters have an optical system to focus this light to a ring image (see Fig. 2) with the aim of distinguishing particles with different masses according to the diameter of the light rings.

The velocity of a particle is given by

$$\beta = \left(1 + \left(\frac{m}{p}\right)^2\right)^{-\frac{1}{2}} , \tag{2}$$

where m and p are its mass and momentum. It is clear from Equ. 2 that the different momenta in a secondary beam with $\Delta p/p \approx 1$ % play little role compared with mass differences of 100 % or more. For two masses m_1 and m_2 one can write

$$\frac{\Delta\beta}{\beta} \approx \beta_2 - \beta_1 = \left(1 + \left(\frac{m_2}{p}\right)^2\right)^{-\frac{1}{2}} - \left(1 + \left(\frac{m_1}{p}\right)^2\right)^{-\frac{1}{2}} \approx \frac{m_2^2 - m_1^2}{2p^2} \tag{3}$$

Figure 3 illustrates the differences of velocity $\Delta\beta/\beta$ corresponding to various pairs of particles with masses m_1 and m_2, as a function of momentum.

Differentiating Equ. 1 with n constant one gets

$$\Delta\theta = \frac{1}{\tan\theta}\,\frac{\Delta\beta}{\beta} \approx \frac{1}{\theta}\,\frac{\Delta\beta}{\beta} , \tag{4}$$

and the difference on the ring radius R, which should allow to separate the particles is given by

$$\Delta R = f\,\Delta\theta = \frac{f}{\theta}\,\frac{m_2^2 - m_1^2}{2p^2} , \tag{5}$$

where f is the focal length of the system. A mechanical diaphragm with variable annular opening, is located in the focal plane to select the photons of the wanted particles. Rings can be distinguished if their radii differ by $\Delta R > LD$, the opening of the light diaphragm. In practice LD can be set as small as 0.1 ± 0.01 mm but it is a difficult optical problem to focus the light to such a sharp ring image.

2.2 Effects broadening the light spot

Various effects must be cured in order to minimize the width of the light rings:

i) Optical aberrations like astigmatism, coma, spherical aberrations are of course existing, but have been minimized and contribute to only 20 μm FWHM in a CEDAR optics. The diffraction limit for a telescope optics with f : 15 and $\lambda = 300$ nm is $d_{min} = 6$ μm and can be neglected.

ii) The most severe effect is the chromatic dispersion which may be expressed as

$$\Delta R_{ch} = f\,\theta\,\frac{1}{2\nu}\,(1 + 1/\theta^2\gamma^2)\,, \qquad (6)$$

where $\nu = \dfrac{n_D - 1}{n_F - n_C}$ is the Abbe number to characterize the reciprocal dispersion of the gas. ($\lambda_D = 589.3$ nm, $\lambda_F = 486.1$ nm, $\lambda_C = 656.3$ nm).

ν must be selected as large as possible and is one of the most important criteria in the choice of the gas.
At high energy the term $1/\theta^2\gamma^2$ in Equ. 6 can be neglected and the chromatic dispersion is directly proportional to θ, which must therefore be chosen as small as possible. In order to improve further their resolution DISC and CEDAR counters have an optical corrector to reduce the chromatic dispersion, (see Ref. 1,2,3 and Chapter 3).

iii) The multiple scattering incurred by the beam during its traversal of the gas radiator also contributes to broaden the light ring. Indeed the centre of the light ring is defined by the direction of the particle trajectory. If this direction changes inside the counter, the photons are spread around non-concentric circles, resulting in a broadening of the spot (see Fig. 4,b). This effect is the most important one when the two previous effects have been corrected, and therefore the radiation length is also a vital parameter to consider in the choice of the gas. The r.m.s. of the light distribution due to the gas scattering is :

$$\sigma_{R(sc)} = f \frac{15}{\beta p} \sqrt{\frac{L \rho P}{3 X_o}} , \qquad (7)$$

where L is the length of the gas radiator, with radiation length X_o, density ρ, and pressure P .

iv) The inhomogeneity of the index of refraction of the radiator contributes to the width of the light rings since

$$\Delta R = \frac{f}{\tan\theta} \frac{\Delta n}{n} , \qquad (8)$$

as from Equ. 1, Equ. 5 and Equ. 4 where $\Delta n/n$ should replace $\Delta\beta/\beta$. In a CEDAR no pressure gradient exists in steady condition, but a temperature distribution may persist for long periods of time, (see Chapter 3). Let us assume a linear variation of temperature along the length L of the radiator, with a gradient $\Delta T/L$. Since $\Delta n/n = -\Delta T/T$ at constant pressure (Equ. 19), the photons will have a rectangular distribution in R with a standard deviation

$$\sigma_{R(T)} = \frac{1}{2\sqrt{3}} \frac{f}{\tan\theta} \frac{\Delta T}{T} \qquad (9)$$

These four effects are incoherent and result in an overwhole worst resolution. The next effect is coherent for any given particle and results in a broadening of the light spot only when averaging is made over many particles.

v) The beam divergence creates another problem since the light rings are concentric only when the particles have parallel trajectories. If not the projected angles x' and y' of a particle trajectory result in a displacement of the centre of the light ring by amounts

$$\Delta x = f\, x' \,, \quad \Delta y = f\, y' \,. \tag{10}$$

Hence the light distribution averaged over many particles is characterized by

$$\left.\begin{aligned} \sigma_{R(x')} &= f\, \sigma_{x'} \\ \sigma_{R(y')} &= f\, \sigma_{y'} \end{aligned}\right\} \tag{11}$$

as illustrated on Fig. 4,d, where $\sigma_{x'}$ and $\sigma_{y'}$ correspond to the beam divergence.

Note that this effect is generally different in the horizontal and vertical planes; furthermore, it does not concern all particles to the same degree since those with small x', y' are not touched and those with large x' or y' are most affected. In other words, a CEDAR counter has an efficiency which decreases with increasing angle between the particle trajectory and the optical axis (see Fig. 5, for a typical example, where the six-fold efficiency is shown and x', y' are scaled in units of LD/f).

vi) Other sources contribute to the background between the particle peaks like the photomultiplier noise, the light produced by halo particles hitting optical components, or the scintillation light produced by beam particles in the gas.

2.3 Choice of parameters

The choice of many parameters of the counter is the result of an overhall optimization of performance made by a computer simulation of the light collection. We are not going to describe this procedure in detail but we just want to recall the physical arguments which were playing against each other.

The number of photons of Cerenkov light emitted is given by[4] :

$$N_{ph} = 2\pi\alpha \, L \, \sin^2\theta \int \frac{d\lambda}{\lambda^2} \quad , \tag{12}$$

where α is the fine structure constant, L the length of the radiator, and the sum extends to the range of wave lengths accepted by the system.

Thus three parameters influence the light output : the Cerenkov angle θ , the length of the radiator and the width of the accepted spectrum, especially towards small wave lengths.

But in order to reach a good velocity resolution the counters need to have, according to Equ. 4,

$$\theta \, \Delta\theta << \frac{\Delta\beta}{\beta} \quad , \tag{13}$$

Now the resolution in θ is merely defined by the chromatic dispersion of Equ. 6 which can be simplified to

$$\Delta\theta_{ch} = \frac{\theta}{2\nu} \quad , \tag{14}$$

when the counter is used at high energy ($\gamma > \frac{1}{\theta}$).

Combining Equ. 13 and Equ. 14, we get

$$\frac{\theta^2}{2k\nu} << \frac{\Delta\beta}{\beta} \quad , \tag{15}$$

where k is the correction factor achieved by the chromatic corrector, and one sees that θ should be small in contradiction with

the light output requirement. To reach a good k one also tends to reduce the spectral range which is detremental to the light output and the length of the radiator is limited for consideration of the beam layout in the experimental halls. The choice of the gases was made in order to minimize the chromatic dispersion (large ν) and the multiple scattering, and with a view on the minimum momentum, p_{min}, which could be achieved within 15 bars (the maximum pressure for which the counter can be operated).

These considerations, together with the optical system which is described in Chapter 3 have lead to the figures summarized in Table I.

The lowest momenta for which the counters can be set to detect particles of mass, m, are given there as a ratio Pmin/m.

Working pressure P and multiple scattering $\langle\theta\rangle_{sc}$ resulting from a full traversal of the counter, are illustrated in Fig. 6 and Fig. 7.

Table I design parameters

CEDAR type	$\frac{\Delta\beta}{\beta}_{sep}$	gas	$(n_o-1)\times 10^6$	ν	θ (mrad)	k	$\frac{\theta^2}{2k\nu}$	L (m)	p_{min}/m
W	5×10^{-6}	N_2	292	35	30.9	11	1.2×10^{-6}	3.24	11.3
N	10^{-6}	He	38.7	54	25.8	24	2.6×10^{-7}	3.88	55.9

2.4 Pattern recognition

The prime aim here is to discard the signal produced by unwanted particles, i.e. rings of a slightly different diameter.

This is best done by collecting the light through a circular diaphragm of variable aperture, LD, and focussing it onto a number of photomultipliers. This number must be large enough to provide a good discrimination against wrong rings of light even when one or two photomultipliers are failing to detect the event. CEDAR counters have got eight photomultipliers, so that the discrimination against unwanted particles is good when at least five photomultipliers are flashing.

The detection of good particles must also have a sufficient immunity against random background as identified in parag. 2.1 vi). For that a high level of coincidence between the photomultiplier signals will also be the best ingredient. Signals with majority counts of eight-fold, seven-fold and six-fold coincidence are provided to the user. The level of coincidence plays an important role in the relation of efficiency to rejection.

2.5 Efficiency and rejection

For a given photomultiplier the efficiency, η, of recording the signal is given by

$$\eta = 1 - e^{-\phi} , \tag{16}$$

where ϕ is the average number of recorded photoelectrons, see Appendix A.

If eight photomultipliers are whatching the same event with similar efficencies, η, then the probability of observing the various levels of coincidence eight, seven and six are given by

$$\left.\begin{aligned} \eta_8 &= (1 - e^{-\phi})^8 \\ \eta_7 &= \eta_8 + 8\,(1 - e^{-\phi})^7\, e^{-\phi} \\ \eta_6 &= \eta_7 + 28\,(1 - e^{-\phi})^6\, e^{-2\phi} \end{aligned}\right\} \tag{17}$$

These values are shown on Fig. 8, where the number of photoelectrons, for a typical operation of a CEDAR, is in the range : $1 < \phi < 4$.

In practice ϕ can be determined experimentally when the CEDAR is set correctly, by counting simultaneously the number of coincidences of various levels: N_6, N_7, N_8. Since these numbers are in direct proportion to the efficiencies η_6, η_7, η_8 their ratios can be substituted for the ratios η_7/η_8 in Equ. A8 and for η_6/η_8 in Equ. A11, and values of ϕ can be calculated.

These values are then used to compute in return the efficiencies for six, seven and eight-fold coincidence levels, through Equ. 17, and the information so obtained is vital for the user to check that the counter keeps in good running conditions.

3. DESCRIPTION OF CEDAR COUNTERS

3.1 Optical system

The optical system of a CEDAR focusses most of the Cerenkov light onto the plane of the diaphragm with the help of a spherical mirror, which constitute the most difficult problem of manufacturing, as explained below. The chromatic dispersion mentioned in para. 2.2, ii) is reduced by a correcting system. For all optical elements the tolerances needed for the quality of the surfaces, for the radii of curvature, for the positioning, tilt and excentricity etc. have been assessed with computer simulation of CEDAR performances.

3.1.1 Chromatic corrector

The most flexible system is a composite lens with quartz and salt rings, which does not deflect the central wave length (see Fig. 9,a). By locating it at various distances to the focal plane, one varies the compensation in relation with the gas pressure. This solution has been adopted at the unique DISC counter[1] made for FNAL but is a complex and expensive system.

If one accepts to use only one kind of gas in a given counter, the chromatic dispersion only depends upon γ of the wanted particle through Equ. 6. Therefore a fixed corrector can be designed to best compensate for the chromaticity when the ultimate resolution must be achieved, i.e. for separation of kaons and pions of the highest momentum. With decreasing momentum (higher gas pressure) the chromatic dispersion gets larger and is only partially compensated by the fixed corrector, but the separation between the light rings increases faster than the spot size as it can be seen from Fig. 10.

This solution has been adopted and in order to cure both transversal and longitudinal chromatic aberrations, two quartz lenses are needed, see Fig. 9. The first lens can be associated with the mirror, which becomes a Mangin mirror, (back surface reflecting), (see Fig. 9,b). This mirror has a central hole of 100 mm diameter to let the beam through. These optical elements are shown in real proportions in Fig. 11.

When the best correction is achieved it still provides only a first order cancellation (the curvature of the dispersion function $n(\lambda)$ is not the same for He and SiO_2, nor N_2 and SiO_2).

Thus a second order dispersion remains, which grows rapidly towards the UV region. To strike a balance between maximum light output and best resolution we have set a cut off at λ = 240 nm by means of glass filters glued onto the exit windows.

3.1.2 Mangin mirror

Strict tolerances have been put on the quality of the quartz blanks (300 mm diameter and 40 mm thickness), in which the mirrors are polished. A path length homogeneity of $\lambda/8$ was required. One unique supplier has offered to produce quartz pieces of such dimensions and quality and the acceptance of these blanks has been subjected to the analysis of double path interferometry in order to qualify the inhomogeneities in terms of spherical aberrations and astigmatism, see Ref. 3. The quality requested was not really met by all the blanks and spherical polishing would not have produced mirrors with the wanted performance. But some aspherical figuring could be done on the back surface of the mirrors to help correcting for the quartz imperfections. As a final test, double traversal analysis with the scatter fringe method was made to check the achieved quality (Fig. 12).

Behind the diaphragm eight simple condenser lenses are focussing the light onto the photomultipliers.

Table II shows the main parameters of these optical elements.

TABLE II

Optical parameter list

	CEDAR-W	CEDAR-N
Mirror		
Glass	Suprasil I	Suprasil I
Outer diameter	300 mm	300 mm
Hole diameter	100 mm	100 mm
Radius of reflecting surface	8610 mm	8913 mm
Radius of refracting surface	6615 mm	8074 mm
Thickness	40 mm	40 mm
Corrector		
Glass	Suprasil I	Suprasil I
Outer diameter	320 mm	270 mm
Hole diameter	150 mm	150 mm
Thickness	20 mm	20 mm
Radius of entrance surface	1385 mm	2885 mm
Radius of exit surface	> 5000 m	> 5000 m
Condensers		
Glass	Spectrosil	Spectrosil
Thickness	10 mm	10 mm
Radius of entrance surface	300 mm	270 mm
Radius of exit surface	∞	∞
Radial excentricity	30 mm	10 mm

3.1.3 Optical tests

For every CEDAR optics the optimum longitudinal positions of the lenses have been computed with the measured radii of curvature. The system was then tested with a light source put at the height of the diaphragm, by collecting the light through a movable slit on the other side of the diaphragm, (Fig. 13). In this process the light is reflected on the test mirror of quality $\lambda/15$ and simulates a Cerenkov emission. This double path through the whole optical system gives a high sensitivity to measure defects or mismatches, which all result in an increase of the spot size. Such measurements allowed us to establish the focal length of the system to within one millimeter and once this information was available another computer optimization was carried out to define the final position of the mirror and of the corrector.

3.1.4 Light output

It is interesting to know that the mirror diametre has not to be made larger than 300 mm, as shown in Fig. 14, for the benefit of off axis particles, since there is no point in collecting more photons in the already favored sectors 1 to 4, as shown for example by the shaded area on (Fig. 15).

The range of the photon spectrum which can be accommodated is surveyed in para. 3.1.1 above and is limited by the needs for high resolution.

The back surface of the mirror is coated by Balzers with Alflex UV covered by a protecting layer and a high reflectivity up to 90 % has been obtained. All refracting surfaces are treated with MgF_2, (a 75 nm thick layer), for a minimum reflection at 300 nm.

A very good transmission efficiency for the total quartz thickness of 120 mm is achieved with Suprasil I and Spectrosil A.

All effects contributing to the effective spectrum are illustrated in Fig. 16.

3.2 Mechanical engineering

The pressure vessel (15 bar) is made of an steel pipe with a diameters 534/558 mm, welded on square flanges to which a nose with eight quartz windows and PM's is bolted on the upstream end whereas a spherical head is closing the downstream end (see Fig. 27).

3.2.1 Temperature uniformity

In order to achieve a temperature uniformity of $\pm$ .1 K as required in the most extreme conditions, (see parag. 3.3.1), the whole counter is packed with 100 mm of polyurhethane foam to provide best thermal insulation. The supporting feet, gas pipes and electric cables are designed to minimize thermal conduction to the outside world. In order to improve the longitudinal conductivity, thick aluminium shells have been clamped to the outside of the big vessel and copper shells are fastened onto the nose. With these improvements the time constant for heat diffusion along the counter is reduced to less than a day and the dayly variations of the external temperature are attenuated by a factor of 20. The vessel temperature is monitored by three Platinum wire thermometers located at both ends and at the diaphragm main flange. Temperature gradients of $\Delta T \geq .3$ K have been monitored only exceptionally after a big seasonal temperature change in the halls.

3.2.2 Windows

The beam is traversing the counter through circular windows with a diameter of 100 mm and a thickness of 0.4 mm made of aluminium alloy (norm AFNOR = AZ5GU). These membranes are hydroformed in hard state to reach a radius corresponding to the equilibrium sphere for the elastic limit of their material. Samples have undergone a life test of 2000 cycles with 1 to 45 bars excursions and a rise time of 0.1 s. The tightness is obtained with all metallic contacts of the membranes on bolted flanges machined with toroidal surfaces.

The eight optical windows are made of quartz cylindres with 45 mm diametre and 10 mm thickness. Their ring frame is made of stainless steel and the binding is obtained by heating the rings at 150°C. When the ensemble is cooled down, a layer of silver is compressed and produces a perfect sealing. A destructive test was made whereby 300 bars were reached.

3.2.3 Optical tower

The supporting structure holding the mirror, the chromatic corrector and the diaphragm is an isostatic triangular assembly of tubes bolted on spherical cups. The tower is straight to within $\pm$ .2 mm over 4.5 m and has a static sag of .1 mm. It is supported by a sphere under the diaphragme and is fixed without constraint to the pressure vessel so that pressure or temperature variations do not affect the optical axis. The ring diaphragme is located at the upstream end of the tower. The mirror frame, fixed at the downstream end, provides for mirror alignment in both radial and longitudinal directions. The chromatic corrector rests on the first intermediate ring of the tower and can also be aligned in three directions.

3.2.4 Ring diaphragm

The diaphragme is composed of a disc with 8 elongated apertures and 8 outer and 8 inner segments moved by right-left screw drive. The segments are bolted on high precision guided chariots. The 8 screw drives are provided with pinions and are turned simultaneously by a gear mounted on ball bearings in a vee-groove on the periphery of the disc (see Fig. 17). The opening can be varied between 0.03 mm and 20 mm in steps of 0.01 mm with a motor located externally to the vessel. A final check of the circularity of the aperture performed on an optical turntable shows radial deviations of less than 0.02 mm.

3.2.5 Alignment table

The fine alignment of the optical axis with the beam axis is made by rotating the whole counter. To provide for this motion the pressure vessel is supported on three points : one sphere located under the diaphragme and two spheres whose bases are resting on a vee-shaped surface. The alignment mechanism made of casted aluminium has two chariots moved by right-left screw drive, opening the vee-surface. The motion of these chariots in opposite direction

produces a vertical displacement whereas a motion in the same direction (horizontal displacement) is provided by another screw drive.

These fine displacements in H and V directions with a step resolution of 0.01 mm provide an angular positioning within 4 μrad.

TABLE III

Mechanical parameter list

Overall	
length	6200 mm
width	920 mm
height	2690 mm
weight	2.4 t
Beam windows	
material	Aluminium alloy
diameter	100 mm
thickness	0.4 mm
Optical tower	
length	4500 mm
sag due to gravity	.1 mm
thermal expansion	.05 mm/K
Diaphragme	
azimuthal opening	8×42.6^{o}
radial opening (LD)	0 to 20 mm
opening accuracy	.01 mm
Alignment table	
x, y range	-4.3 to +4.3 mm
Δx, Δy accuracy	.01 mm
angular resolution	2.3 μrad

3.3 Gas controls

In order to achieve the best mass resolution, the index of refraction must be uniform in the whole radiator and stable during the period of data taking. The first condition requires an excellent uniformity of temperature which is obtained by the means explained in parag. 3.2.1 above, but it does not imply that this average temperature has to be kept constant in time. The second condition requires a perfect tightness of the vessel and/or an easy way of restoring the wanted index of refraction, by tuning the pressure to follow the volume variations of the vessel due to temperature changes.

3.3.1 Measurement of the index of refraction

The variations of the index of refraction must be kept, say, ten times smaller than the ultimate resolution $\frac{\Delta\beta}{\beta} = 10^{-6}$, in order to match the quality of the optical system. One therefore aims at keeping the index of refraction within $\frac{\Delta n}{n} \leq 10^{-7}$. Although it is possible to build a refractometer with this resolution (see Ref. 4), it was not felt desirable to have refractometers of that quality and complexity attached to each of the twelve CEDAR counters operating in the SPS areas. It was instead chosen to monitor the density of the gas through pressure and temperature. Indeed the index of refraction can be deduced from the density since a unique gas is used with each type of counter.

The index of refraction of a gas can be expressed in terms of electron oscillators as :

$$n - 1 = \frac{N\, q_e^2}{2\, \varepsilon_o\, m} \sum_K \frac{f_k}{\omega_k^2 - \omega^2 + i\, \gamma_k \omega} \quad , \tag{18}$$

where N is the number of atoms per unit volume, see Ref. 5. Clearly $n - 1$ is proportional to the gas density and, using the perfect gas equation, this can read :

$$n - 1 = (n_o - 1) \left(\frac{To}{Po}\right) \frac{P}{T} \quad , \tag{19}$$

where P and T are the actual pressure and temperature and n_o is measured at $P_o = 1$ bar and $T_o = 293$ K.

The error propagation obtained by differentiation of Equ. 19 reads :

$$\frac{\Delta n}{n} = \frac{(n-1)}{n}\left[\frac{\Delta P}{P} - \frac{\Delta T}{T}\right]. \qquad (20)$$

Since $\frac{n-1}{n} \approx \frac{1}{3000}$, (see Table IV), the accuracy needed to monitor P and T is 3000 times less than the accuracy requested to measure directly n .

Tolerances on n , P and T corresponding to the wanted resolutions are listed in Table IV below.

TABLE IV

Tolerances and accuracies for gaseous state

CEDAR type	θ (mrad)	$\frac{n}{n-1}$	Ultimate separation $(\Delta\beta/\beta)_{sep}$	Corresponding accuracies			
				$\Delta\beta/\beta$	$\Delta n/n$	$\Delta P/P$	ΔT
W	30.9	2095	5×10^{-6}	5×10^{-7}	5×10^{-7}	10^{-3}	0.3 K
N	25.8	3005	10^{-6}	10^{-7}	10^{-7}	3×10^{-4}	0.1 K

In practice the measurement of the temperature is straightforeward but the precautions explained en Chapter 3.2. are needed to obtain a uniformity of temperature along the vessel. To measure the pressure a precise instrument is required, which is calibrated in the laboratory with a reference refractometer.

The slight contamination of the gasses (N_2 or He), due to leaks of the windows or coming from outgassing of the counter vessel can be dealt with.

3.3.2 Gas pressure monitoring and absolute calibration

The heart of the pressure control is a very accurate pressure transducer[6] which provides an electrical wave form with a stability of 10^{-4} and whose frequency is related to the pressure of the gas (so that a measurement of pressure is reduced to a measurement of a frequency). The principle of operation of these transducers is briefly illustrated below. The sensing elements consist of two concentric cylinders, a vibrating inner one and a protective outer one. A spool body internal to the inner cylinder holds small electromagnets which drive the vibrating cylinder and pick-ups to detect its motion and frequency. The space between the two cylinders is evacuated to give an absolute pressure reference. The volume between the inner cylinder and the spool body is pressurized with the gas to be measured and this causes the cylinder natural frequency to increase. The frequency is detected by the pick-up which provide a square wave voltage whose frequency is proportional to the pressure of the gas.

The whole transducer is thermostatized at $40 \pm 0.5^{o}C$ in order to avoid the frequency swing due to external temperature.

Each pressure transducer is calibrated[7] by means of a Rayleigh-type refractometer in the laboratory. For each pressure point the index of refraction is established by counting the fringes for the optical path difference between an evacuated cell and a cell filled with the gas for which pressure and temperature are recorded simultaneously. A typical number of fringes is ten thousands and the high accuracy is obtained by sharp interpolation by means of an array of sixteen light diodes.

The frequency response of the Hamilton transducer is not linear in pressure and a fit is made for each transducer of a polynomial with six parameters[7].

3.3.3 Gas handling

Each CEDAR is connected to the gas supply network of nitrogen or helium, where a pressure of 20 bar is available. On the feeding line the pressure is automatically kept at a value $P + \frac{0.5}{P}$ with a spring biased pressure regulator. Similarly a pressure of P_o 0.5 is maintained on the outlet branch so that equal quantities of gas can be let in or out by activating on/off valves for a controlled time. In this way the gas pressure can easily be computer controlled. A gas expansion of less than 0.5/P at the inlet is important to keep the temperature uniformity needed for the best resolution (see parag. 5.3,vi).

4. LAY-OUT, ELECTRONICS AND COMPUTER CONTROLS

4.1 Lay-out

The angular acceptance of CEDAR counters is very small when the light diaphragm is closed to insure best separation. Therefore the SPS beam have been designed with a very parallel section (large beam dimensions and small divergence in both H and V-planes) for the installation of CEDAR counters, in order to optimize the counting efficiency.

One or two CEDAR counters can be installed in such sections and the basic lay-out, shown in Fig. 18, consists of :

- 2 scintillation counters XTRI 1, XTRI 2 (Ø 100 mm, 5 mm thick NE 110),
- 1 anticounter XANT (with a circular hole of Ø 100 mm) in front of each CEDAR,
- 1 two-plane (horizontal and vertical) analog wire chamber XWCA[8],
- 2 pairs of filament scintillation counters[9] XFS.

The two XTRI are used in coincidence to define the useful beam region. The counters XANT are used to veto halo particles which travel outside the useful beam (their use is recommended when working at beam intensities of 5×10^6 or more). The wire chambers XWCA are used to measure the beam position and size at the CEDAR during the tuning of the beam. The two pairs of XFS (horizontal and vertical filament beam scanners) are finally used to adjust the beam direction and parallelism, by operating them in coincidence[9].

The trigger counters, the wire chamber and the scintillator filaments of the XFS's must be taken out of the beam during data taking, (remote control).

4.2 Electronics for signal treatment

The block diagram of the electronics associated to each CEDAR is shown in Fig. 19.

The signals from the 8 photomultipliers are first shaped by fast discriminators operated at low threshold to detect one single photoelectron, and then split into two ways.

One way is sent to a majority state logic unit where three levels of coincidence (6, 7 and 8-fold) are provided and sent to the experimenters, usually in anticoincidence with the XANT signal.

A parallel output of the discriminators is used for the diagnostics of the instrument. The signals of each photomultiplier are sent to a strobed coincidence unit and recorded on 8 scalers. When the two XTRI trigger counters are introduced in the beam, their coincidence signal is used as strobe input, the counts read in the 8 scalers give information on the efficiency of each photomultiplier and on the size and position of the light ring image at the diaphragm plane.

To complete the CEDAR diagnostics, the counts of the 6, 7 and 8-fold majorities are also recorded ; they are used to evaluate the average number of photoelectrons NPE seen by the photomultipliers, (NPE is deduced from the ratio of the rates counted at the three levels of coincidence, see Appendix A), and to measure the mass spectra and the rejection of unwanted particles while scanning the CEDAR gas pressure.

4.3 Computer controls

All CEDAR counters installed in the SPS secondary beams can be operated simultaneously from the EA computer terminals installed in the experiments counting rooms via a set of control and diagnostic programmes.

A series of interacting programmes has been written to help in tuning and operating each CEDAR. They can be run under the TREE associated to the beam line in use. The sequence and the several options are listed below :

```
#TRUNK#  ---/---/---/DETECTORS///---/BACK : DET
#DETECT# CEDAR/---/---/----------------/  : CEDAR
#CEDAR#  STATUS/SETUP/TUNE/MEASURE-----/BACK
                |      |      |
                |      |      |_______| EFFICIENCY
                |      |              | SCAN
                |      |
                |      |  PRESS
                |      |  MASS
                |      |__DIAPHRAGM
                |         ALIGNMENT
                |
                |__ TRIGGERS
                    PMS
```

A description of the subroutines is given in the following. The algorithm used is as collected in Appendices A and B.

STATUS : is an acquisition programme which reads and displays the parameters of the detector useful to its control and operation. A typical example of its write-out is shown.

```
# DETECT # CEDAR/THRESH/MWPC/FISC/TRIG/SPECTR/ATRIG/HODOSC/SPILL/EXPT/:CEDAR

         CEDAR IN THIS BEAM: 2
         NUMBER :1

# CEDAR # STATUS/SETUP/TUNE/MEASURE/////BACK/:ST

STATUS OF #    CEDAR - 1 # IN BEAM H6 AT -150 GEV/C     1982-04-28-21:08
*****************************************************************************

# GAS TEMPS #    HEAD =  22.50 [DEG]  \
                 MID  =  22.35 [DEG]   >   MAX. TEMP. DIFF.=  .30 [DEG]
                 TAIL =  22.20 [DEG]  /
                 TRANSDUCER IS OK =  39.47 [DEG]    ROOM =  23.49 [DEG]

# PRESS AND MASS #  PRESS= 10.3270 [BAR]   MASS=  .469  +/- .003  [GEV]

# MASS-PRESS #            ELECTRONS=10.170 [BAR]  MUONS  =10.185 [BAR]
      PIONS=10.191 [BAR]  KAONS    =10.343 [BAR]  PROTONS=10.776 [BAR]
# MOTORS POS. #
       DIAPHRAGM= 1.00 [MM] * HOR. X =  .00 [MM] * VERT. Y =  .30 [MM]

# TRIGGERS POS. #     TRIGGERS ARE IN          HV IS ON

# PMS #   EFF'S (6)=9.60E-1    EFF'S (7)=8.10E-1    EFF'S (8)=4.26E-1
          TRIGGERS =2.38E6    NPE/PM =2.29
*****************************************************************************
   HARDCOPY  (Y/RET):
```

#GAS TEMPS# gives the gas temperature in three sections of the vessel; their average value is used with the gas pressure to evaluate the actuel index of refraction of the radiator.

The body temperature of the pressure transducer (Section 3.3) is also given. A warning message is issued in case of abnormal value since in that condition the transducer information is wrong.

╫PRESS AND MASS╫ gives the actuel average gas pressure and the value of the mass on which the detector is presently tuned.

╫MASS-PRESS╫ gives the gas pressures which should be used, accordingly with the actual gas temperature, to tune the CEDAR on the masses of e, μ, π, k and p for the current beam momentum.

╫MOTOR POS╫ gives the light diaphragm opening and the position (horizontal and vertical) of the alignment table.

╫TRIGGER POS╫ checks the position of the triggers in the beam and if their high voltage is ON or OFF, without modifying any of these parameters.

╫PMS╫ evaluates the 6, 7, 8-fold efficiencies from the measured average number of photoelectrons per PM (NPE) -Appendix A- and from the beam intensity (TRIGGERS).

SETUP reads and displays the parameters (delay and PM high voltage) of the triggers associated to the CEDAR (TR) and those of the CEDAR itself (PMS). Both subroutines allow to switch OFF the PM's H.V. or to restore them to the reference values. The TR branch also permits to take the triggers out of the beam, when the CEDAR is ready for data taking.

```
#SETUP#   :TRIGGERS/PMS/ :TR

TRIGGERS OF CEDAR - 1 # IN BEAM H6 AT -150 GEV/C        1982-04-28-21:10
*******************************************************************************

#POS. TRIGGERS # TRIGGERS ARE IN

 TRIGGER      DELAY[NS]    HV[KV]     SCALER
  UPSTR          -1          1.82      2.17E6
 DOWNSTR         29          1.91      2.15E6

TRIGGERS # WANT THEM IN BEAM (Y/N):Y


# TRIGGERS PMS # RESTORE/ZEROHV (R/Z):
```

```
#SETUP#   :TRIGGERS/PMS/ :PMS

PMS CEDAR - 1 # IN BEAM H6 AT -150 GEV                  1982-04-28-21:11
*******************************************************************************

# TRIGGERS POS. # TRIGGERS ARE IN


PM NUMBER        DELAY[NS]     HV[KV]     SCALER
    1              0           1.71       5.79E5
    2             11           2.51       5.66E5
    3             10           2.10       5.20E5
    4              6.5         1.74       3.31E5
    5             15           2.01       5.51E5
    6              8           2.40       8.73E5
    7             12           2.20       1.00E6
    8             14           2.21       9.02E5
6-FOLD             0          *****       1.14E5
7-FOLD             7          *****       9.49E4
8-FOLD             0          *****       5.04E4
TRIGGERS-COINC     0          *****       2.46E6

# CEDAR PMS # RESTORE/ZEROHV (R/Z):
```

TUNE is an active programme by which allows to tune the CEDAR through the routines :

PRESS/MASS/DIAPHRAGM/ALIGNMENT

- PRESS : The current gas pressure is measured, then a different value in the permitted range can be requested. The new value is measured at the end of the operation. The write-out is self-explanatory.

- MASS : The mass which could be detected with the current value of the index of refraction is evaluated (Appendix B) together with its uncertainty, then a new value can be asked for. The write-out is similar to PRESS.

- DIAPHRAGM : Same as for previous routines.

- ALIGMENT : Allows to align the optical axis of the detector on the average beam direction. This is achieved by using the XY alignment table (Section 3.2.5) which supports the downstream end of the counter. The range of displacement of the XY table is ± 4.5 mm with an accuracy of 0.02 mm in both directions, which allows to move the CEDAR optical axis inside a cone of 1 mrad semi-aperture with an accuracy of 4 μrad to get the best matching with the beam direction. A typical print-out of this routine is shown below.

```
ALIGNMENT CEDAR - 1 - IN BEAM H6 AT -150 GEV/C          1982-04-28-21:23
*******************************************************************************
# TRIGGERS POS. # TRIGGERS ARE IN


PRESS=18.3278 [BAR]      MASS =  .469  +/-  .003  [GEV]

TRIGGERS = 2.05E6        NPE/PM= 2.29

                    DIAPHRAGM =  1.00 [MM]
                    HOR  X    =  1.00 [MM]
                    VERT Y    =   .30 [MM]

      % PM/TRI                                    2 PM /MEAN
      *********                                   **********
                                                      (U)
8      35   24       1                               109
7    42       24     2        R/L =  .61
6    34       22     3        U/D = 1.66      (L)  139      85  (R)
5     21   14       4                                 65
                                                      (D)


CHANGE ALIGNMENT (YES/RET)
```

First, the two triggers are positioned in the beam and the actuel status of the detector is given (gas pressure and motor positions).

The counting rate of the eight PM's, normalized to the beam intensity (TRIGGERS) are then displayed from 1 to 8 following their position on the counter (beam entering the screen).

The ratios

$$\frac{R}{L} = \frac{2 + 3}{6 + 7} \quad , \quad \frac{U}{D} = \frac{1 + 8}{4 + 5}$$

are shown in the central part, while in the right part of the screen the eight counting rates are grouped (R = 2 + 3, etc.) and normalized to the average of them all.

```
ALIGNMENT CEDAR - 1 - IN BEAM H2 AT  250 GEV/C          1981-09-25-11:59
*************************************************************************

8   38  36   1    CEDAR #1  H2  250 GEV * TRIG= 3.94E5     * 2 PM/MEAN *
7 76      70 2    U/D = 2.93  R/L = 1.01  NPE/PM=  .76          85
6 46      54 3    X =  -.84*Y =  2.79*DIA =   .29 [MM]     141       143
5   9  16   4    M=  .932 [GEV] - 1- P= 10.4131 [BAR]           29
*************************************************************************
8   69  66   1    CEDAR #1  H2  250 GEV * TRIG= 3.79E5     * 2 PM/MEAN *
7 77      73 2    U/D = 1.79  R/L = 1.03  NPE/PM= 1.31          113
6 54      62 3    X =  -.84*Y =  2.90*DIA =   .29 [MM]     109       113
5  30  45   4    M=  .932 [GEV] - 2- P= 10.4131 [BAR]           63
*************************************************************************
8   77  73   1    CEDAR #1  H2  250 GEV * TRIG= 1.78E5     * 2 PM/MEAN *
7 75      73 2    U/D = 1.34  R/L = 1.12  NPE/PM= 1.66          112
6 52      70 3    X =  -.84*Y =  2.95*DIA =   .29 [MM]      95       107
5  44  67   4    M=  .932 [GEV] - 3- P= 10.4131 [BAR]           84
*************************************************************************
8   78  76   1    CEDAR #1  H2  250 GEV * TRIG= 3.74E4     * 2 PM/MEAN *
7 72      73 2    U/D = 1.12  R/L = 1.10  NPE/PM= 1.89          109
6 56      69 3    X =  -.84*Y =  2.99*DIA =   .29 [MM]      91       101
5  61  76   4    M=  .932 [GEV] - 4- P= 10.4131 [BAR]           97
*************************************************************************
8   79  77   1    CEDAR #1  H2  250 GEV * TRIG= 3.07E5     * 2 PM/MEAN *
7 75      74 2    U/D = 1.12  R/L = 1.08  NPE/PM= 1.93          108
6 59      70 3    X =  -.84*Y =  3.01*DIA =   .29 [MM]      93       101
5  62  76   4    M=  .932 [GEV] - 5- P= 10.4131 [BAR]           96
*************************************************************************
8   79  78   1    CEDAR #1  H2  250 GEV * TRIG= 3.01E5     * 2 PM/MEAN *
7 73      75 2    U/D =  .99  R/L = 1.06  NPE/PM= 2.12          104
6 65      72 3    X =  -.84*Y =  3.05*DIA =   .29 [MM]      91        98
5  75  82   4    M=  .932 [GEV] - 6- P= 10.4131 [BAR]          104
*************************************************************************
8   79  77   1    CEDAR #1  H2  250 GEV * TRIG= 1.65E5     * 2 PM/MEAN *
7 75      72 2    U/D =  .98  R/L =  .96  NPE/PM= 2.15          103
6 70      69 3    X =  -.90*Y =  3.05*DIA =   .29 [MM]      96        93
5  77  81   4    M=  .932 [GEV] - 7- P= 10.4131 [BAR]          105
*************************************************************************
8   79  78   1    CEDAR #1  H2  250 GEV * TRIG= 2.46E5     * 2 PM/MEAN *
7 73      73 2    U/D =  .98  R/L = 1.02  NPE/PM= 2.14          104
6 67      71 3    X =  -.87*Y =  3.05*DIA =   .29 [MM]      93        96
5  76  82   4    M=  .932 [GEV] - 8- P= 10.4131 [BAR]          105
```

MEASURE allows to measure the CEDAR efficiency and to perform a pressure scan (SC) to better define the right working point.

- EFFICIENCY displays the measured 6, 7, 8-fold counting rates normalized to the beam total intensity (TRIGGER); the related efficiencies evaluated as described in Appendix A are then shown.

- SCAN offers the choice between a pressure scan or a light diaphragm scan at a given gas pressure.

P-SCAN is a programme which performs a gas pressure scan between two given limits and with a given number of steps. After every step the six, seven and eight-fold majorities are acquired but the display is given only when the required statistics (TRIG) has been reached.

The number of photoelectrons NPE per PM is evaluated from the three majorities (see Appendix A) and it is quoted together with the ratio R between the two results for NPE which should be $\sim$ 1 in case of good statistics.

A typical print-out is shown in the following, where the gas pressure scan has been performed decreasing the CEDAR pressure in order to perturb as little as possible the thermal equlibrium of the gas. The scan limits have been chosen in order to locate the K^+ and π^+ peaks.

The slight differencies between the pressure values corresponding to the peaks and the theoretically predicted ones are due to changes in the gas purity and can be duly corrected.

CEDAR# 1 IN BEAM H2 SCAN FROM 10.2755 TO 10.26 [BAR] 1981-09-24-16:45
DIAPHRAGM = .29 [MM] MOMENTUM: .250 GEV/C STEP= -1.75 [MBAR]

MEAS #	PRESS [BAR]	TRIG	NPE/PM	R	--------MAJORITIES-------- 6-FOLD	7-FOLD	8-FOLD	CYCLE #
1	10.2762	5.01E4	1.90	1.06	5.58E-2	3.70E-2	1.60E-2	1
2	10.2748	4.93E4	2.00	1.06	5.43E-2	3.74E-2	1.73E-2	1
3	10.2731	5.14E4	2.00	1.06	5.56E-2	3.81E-2	1.76E-2	1
4	10.2714	5.06E4	2.07	1.06	5.68E-2	4.00E-2	1.94E-2	1
5	10.2704	5.08E4	2.03	1.04	5.75E-2	4.14E-2	1.92E-2	1
6	10.269	5.10E4	2.10	1.05	5.63E-2	4.11E-2	2.01E-2	1
7	10.2676	4.79E4	2.10	1.05	5.79E-2	4.23E-2	2.07E-2	1
8	10.2662	4.97E4	2.11	1.05	5.81E-2	4.27E-2	2.10E-2	22
9	10.2652	4.88E4	2.04	1.05	5.91E-2	4.23E-2	1.98E-2	1
10	10.2642	4.87E4	1.97	1.03	6.05E-2	4.28E-2	1.91E-2	1
11	10.2625	4.75E4	2.00	1.06	5.75E-2	3.98E-2	1.83E-2	1
12	10.2611	4.87E4	1.93	1.06	5.84E-2	3.91E-2	1.72E-2	1
13	10.26	4.91E4	1.86	1.06	5.77E-2	3.72E-2	1.57E-2	1
14	10.2583	5.03E4	1.86	1.07	5.36E-2	3.38E-2	1.44E-2	1
15	10.257	5.02E4	1.76	1.07	5.49E-2	3.29E-2	1.29E-2	1

P { 6, 7, 8

(P = K+ Peak)

PRESSURE SCAN

LD-SCAN is a programme which scans the light diaphragm opening while sitting on a fixed gas pressure, thus operating the counter like a threshold one.

The display is the same as from the pressure scanning subroutine and it can be used to determine the maximum opening for the light diaphragm to avoid counting unwanted particles while allowing the best possible efficiency.

A typical write-out is given below where the light diaphragm of the CEDAR sitting on K's is opened step by step until light from π's and finally from p's can be registered by the PM's.

5. PRACTICAL OPERATION

When a new experiment is setting up, EA experts help putting the CEDAR(s) in condition to operate and at the same time instruct the users how to do it themselves.

5.1 Particle separation and CEDAR resolution

The separation in millimeters of Cerenkov light rings at the light diaphragm is shown as a function of the beam momentum and for various particles in Figures 20 and 21. In order to get a good particle identification, this separation must be larger than the width of the light rings for which the two main contributions are also shown in Figs 20, 21.

Example : for a CEDAR-N set on kaons at 200 GeV/c one reads from Fig. 21 a light spot of 46 μm, a multiple scattering effect of 85 μm and a distance to the pion ring of 400 μm so that a LD opening between 200 μm and 400 μm would be adequate.

Closing the light diaphragm gives a better rejection of the unwanted particles but a worse efficiency of counting the good ones, especially, in presence of beam divergence.

5.2 Efficiency

Counting efficiencies depend upon various factors : status of optics and of photomultipliers, LD opening, gas pressure and beam momentum, angle of the particle trajectory (due to beam divergence and CEDAR alignment), and choice of the coincidence levels 6, 7 or 8-folds. The average number of photoelectrons, NPE, seen by a PM is related to the counting efficiencies by the relation given in Appendix A and shown on Fig. 8. The 6-fold reaches a high efficiency already with NPE = 2, whereas the 8-fold hardly goes beyond 60 % for NPE $\leq$ 3. Typical numbers of photoelectrons are between 2.5 and 3 for a CEDAR-N and between 3 and 3.5 for a CEDAR-W, with LD wide open. Past experience indicates that the 6-fold has a rejection power good enough for practically all applications encountered so far (one exception is documented in parag. 5.6).

The average efficiency is also dropping when the beam divergence is larger than the angular acceptance of the counter, given by the LD setting divided by the focal length. At very high energy, where one might have to close the LD to 0.1 mm the acceptance is 0.1 mm/3.88 m = 26 μrad for a CEDAR-N. Keeping a beam parallel to this level of precision requires a lot of attention. In the best case there will always be some tail in the divergence distribution for which the counting efficiency is lower.

As an indication of the efficiencies one can reach in practice, we give in Table VI the measured values obtained in an experiment which measured absolute values of target yields[10] with 400 GeV/c protons. The H2 beam had been carefully optimized for those CEDAR measurements.

TABLE VI

Efficiency of CEDARs as measured in Ref. 10.

Energy, polarity (GeV/c)	p_T (GeV/c)	C1			C2		
		LD (mm)	Efficiency (%)	Number of points	LD (mm)	Efficiency (%)	Number of points
-60	0 0.5	0.62 2.52	85.2 ± 0.6 96.6 ± 0.3	3 3	0.62 2.52	66.6 ± 0.6 93.7 ± 0.15	3 3
+60	0 0.5	2.52	96.9 ± 0.3	6	2.52	94.0 ± 0.5	6
-120	0 0.3 0.5	1.24	95.7 ± 0.18	9	1.24	92.5 ± 0.23	9
+120	0 0.3 0.5	1.24	94.85 ± 0.27	9	1.24	91.13 ± 0.54	9
-200	0 0.5	0.23 0.23	80.0 ± 1.8 66.2 ± 2.0	3 3	0.23 0.23	69.5 ± 1.5 71.8 ± 3.3	3 3
+200	0 0.5	0.31	86.71 ± 1.3	3	0.25 0.31	78.34 ± 0.5 77.6 ± 1.0	3 3
-300	0 0.5	0.13 0.13	58.2 ± 0.3 56.2 ± 1.5	3 3	0.13 0.13	50.6 ± 0.4 48.9 ± 1.5	3 3
+300	0.5	0.13	64.5 ± 1.0	3	0.13	56.5 ± 0.5	3

5.3 Procedure for tuning and setting-up a CEDAR

i) The parallelism of the beam must be tuned to provide a beam divergence smaller than the counter acceptance, see para. 5.2.

ii) In order to insure an easier operation of the trigger counters and of the CEDAR during the tuning, better keep the beam intensity below, say, 10^6/s by collimating the beam size without altering the beam divergence at the CEDAR.

iii) Print the STATUS of the CEDAR to check its current pressure, temperatures, etc. and to read the nominal values of pressure corresponding to the different particles. Then set the pressure for the most abundant particle (protons in a positive beam, pions in a negative one).

iv) Open the diaphragme (LD = 20 mm), using the programme ALIGN, to measure NPE and to check that all PM's are efficient : the ratios PM/trigger should all be about 90 %, (if the beam energy is high enough so that all the light rings of π, k and p are falling inside the diaphragme opening (Figs 20 and 21). The ratios of PM efficiencies right/left (R/L) and top/bottom (T/B) obtained with the open diaphragm are to be kept as reference.

v) Align the CEDAR in the beam in order to optimize its performances. This is achieved by trying to reproduce the same values of R/L and T/B after a reduction of the diaphragme opening. Better take a few steps to go to the wanted LD, since the alignment gets more and more tricky with smaller diaphragmes! The real optimum is reached when the values R/L and T/B are the same as for the wide open diaphragme (point iv) above) and the NPE is simultaneously at a maximum. One should not worry if the efficiencies of the right and left PM's (2, 3, 6, 7) are not

the same as the efficiencies of the top and bottom ones (1, 4, 5, 8), this could be due to different beam divergences in the horizontal and vertical planes. But if the overall efficiency is well below what would expected for the particle on which the alignment is done something more fundamental should be checked like the pressure.

vi) The nominal pressures given by the programmes might be slightly wrong due to a gas pollution by air or vessel outgassing. A pressure scan is the best way to check the correct pressure setting. This is a lengthy procedure if one intends to go through several particles peaks, because at low momentum the big change of pressure is time consuming, and at high momentum the good resolution can only be achieved with a perfect thermal equilibrium in the gas radiator. When the vessel pressure is increased by a gas inlet there is an overall adiabatic temperature increase plus a local inlet of cool gas (expansion at the valve). The latter effect is dangerous because of the long time constant (about one hour) needed to reach thermal equilibrium, which is due to the length of the counter. But when a gas outlet is made, there is only a general decrease of temperature followed by an equilibrium reached with a time constant of 15 seconds. Therefore, with $\Delta P = -3$ mbar between points an accuracy of 1 mbar would be reached only if one waits 15 s before each mesurement. A scan done at a higher speed will neither reach the ultimate resolution (best dip between peaks) nor give the exact pressure to 1 mbar accuracy).

In summary a pressure scan should be done by decreasing the pressure, with an LD setting smaller or equal to the distance from the nearest particle peak (see Figs 20 and 21) and with a number of points large enough to get a small ΔP between two measured points. Points are currently measured every two cycles of the SPS with a time interval of typically 24 s.

As an example Figs 20 and 21 show a pressure scan around the π and k peaks, made with two different values of LD. Only the 6-fold majority signal is plotted since it is most in use, except for some special cases (see parag. 5.6).

vii) Fine tuning of the LD. If the particle separation is not sufficient, close slightly the LD and make another pressure scan. If instead it is more than sufficient, but for some reason, especially large beam divergence at the CEDAR, the efficiency is low, then a LD-scan will prove useful to optimize the LD value. Set the pressure on the selected particle peak (measured as in point vi) and then ask a LD-SCAN from say 0.05 mm to twice or three times the particle separation. The output, when conveniently plotted (see Fig. 24), will give a hint on efficiency and rejection of the CEDAR at any LD setting. In fact, the wide LD setting of Fig. 23 has been decided after doing first the pressure scan with smaller LD, also shown in Fig. 22, and then the LD scan shown in Fig. 24. In this particular case the beam divergence was 50 μrad FWHM in the vertical plane and 120 μrad in the horizontal plane.

5.4 Monitoring the CEDAR stability

The monitoring of the index of refraction is a bit more delicate since it does not depend only upon pressure, but also upon temperature (in fact, upon P/T, see parag. 3.3.1). The programme MASS is meant to help there : just keep the wanted mass and restore it using the programme if the value has shifted.

When operating at the utmost resolution, it is necessary to make a pressure scan to check the centre of the peak as indicated in parag. 5.3 vi) above. The gas pressure at the centre of the peak corresponds to a value of mass (read via the MASS or STATUS programmes) slightly off the known particle mass, because the gas purity is never perfect. This fictitious mass value is to be kept during data taking.

5.5 Operation at high beam intensity

CEDAR's set on minority particles have been operated satisfactorily in beams with total intensities exceeding 5×10^7 particles/second. As mentioned in parag. 5.1 such intensities are often achieved by sacrifying somewhat the beam parallelism at the CEDAR, so that the counting rate of the individual PM's can be much larger than the rate of the wanted particles. Even under those conditions the PM's do tolerate single counting rates of 10^7 counts per second. The efficiency depends strongly on the relative values of LD and beam divergence.

5.6 Selection of electrons and muons

Electrons and muons are often used for calibration purposes, in hadron beams.

A CEDAR-N can separate electrons from pions up to 60 GeV/c - but then the use of the 8-fold coincidence is necessary, see Fig. 25. At lower energies, of course, the separation becomes easier, one may use the 6-fold and also a CEDAR-W. Figures 20 and 21 will help in assessing the performance at a given energy.

The same can be said for the separation of muons : Fig. 26 shows a CEDAR-N scan in which electrons, muons and pions are well separated in a 20 GeV/c beam.

APPENDIX A

Statistics of pattern recognition

Assuming that the number of photoelectrons detected by a photomultiplier follows a Poisson distribution the probability of missing an event is

$$P_{\phi}(o) = e^{-\phi} \tag{A1}$$

where n is the average number of photoelectrons, and

$$P_{\phi}(k) = \frac{e^{-\phi}\,\phi^{k}}{k!} \tag{A2}$$

is the general term of the distribution.

Of course, the efficiency of one photomultiplier which detects on average ϕ photoelectrons is

$$= 1 - P_{\phi}(o) = 1 - e^{-\phi} . \tag{A3}$$

When eight photomultipliers are looking at the same event with equal efficiencies η and equal chance of not seeing it, say, $\varepsilon = 1 - \eta$ then the probabilities of various levels of coincidence can be seen from the binomial expansion:

$$(\eta + \varepsilon)^8 = \eta^8 + 8\,\eta^7\varepsilon + 28\,\eta^6\varepsilon^2 + 56\,\eta^5\varepsilon^3 + 7e\,\eta^4\varepsilon^4 + 56\,\eta^3\varepsilon^5 +$$

$$28\,\eta^2\varepsilon^6 + 8\,\eta\varepsilon^7 + \varepsilon^8 . \tag{A4}$$

The first term in the right hand side of Equ. A4 is the probability of the eight photomultipliers flashing (eight coincidence level), the next term is for seven and only seven, the next term is the probability of six and only six p.m. flashing, etc. So that one can write the following probabilities for different levels of coincidence :

$$\left.\begin{aligned} \eta_8 &= \eta^8 \\ \eta_7 &= \eta_8 + 8\,\eta^7\varepsilon \\ \eta_6 &= \eta_7 + 28\,\eta^6\varepsilon^2 \\ \eta_5 &= \eta_6 + 56\,\eta^5\varepsilon^3 \end{aligned}\right\} \qquad \text{(A5)}$$

From measured values of these coincidence levels one can deduce the average number of photoelectrons for the wanted particles ϕ as follows:

$$\frac{\eta_7}{\eta_8} = 1 + 8\,I\,, \qquad \text{(A6)}$$

where $I = e^{-\phi}/(1 - e^{-\phi})$, and conversely

$$\phi = \ln\,(1 + I) - \ln\,I\,. \qquad \text{(A7)}$$

And from Equ. A6 and A7 one has

$$\phi = \ln\left[1 + \frac{8}{\eta_7/\eta_8 - 1}\right]. \qquad \text{(A8)}$$

Similarly with η_6 one can write

$$\frac{\eta_6}{\eta_8} = 1 + 8\,I + 28\,I^2\,, \qquad \text{(A9)}$$

and solving for I gives:

$$I = \frac{-2 + \sqrt{4 - 7\,(1 - \eta_6/\eta_8)}}{14}\,, \qquad \text{(A10)}$$

and finally, using Equ. A7 one gets

$$\phi = \ln\left[1 + \frac{14}{\sqrt{4 - 7\,(1 - \eta_6/\eta_8)} - 2}\right]. \qquad \text{(A11)}$$

The two values given by Equ. A8 and Equ. A11 are used for a consistency check.

APPENDIX B

Algorithm for computer control of the index of refraction

The following symbols are used :

σ, P, T = density (g/cm^3), pressure (bar), absolute temperature (K) of gas

p, m = momentum (GeV/c) and rest mass (GeV) of detected particle

a = gas constant (cm^3/g) for a given light wavelength

$k(\lambda)$ = " " (K/bar) " " " " "

Θ = Cerenkov angle

n = index of refraction of CEDAR radiator.

1. Basic relations

From the definition of Cerenkov angle, the refractive index is

$$n = \frac{1}{\beta \cos \Theta} = \frac{\sqrt{1 + (m/p)^2}}{\cos \Theta} \qquad \text{(B1)}$$

and assuming a linear dependence of n on gas density we have

$$n - 1 = a \rho = k \frac{P}{T} \qquad \text{(B2)}$$

Given the angle Θ^* defined by the optics of the instrument we can derive from (B1) and (B2) the gas pressure needed to detect a particle of mass m and momentum p

$$P = \frac{T}{k} \left(- 1 + \frac{\sqrt{1 + (m/p)^2}}{\cos \Theta^*} \right) \qquad \text{(B3)}$$

Conversely, for any set of values of p, T and P we can compute a mass m which satisfies the relation

$$m = p \sqrt{- 1 + \cos^2 \Theta^* \left(1 + k \frac{P}{T} \right)^2} \qquad \text{(B4)}$$

From (B3) a lower limit for gas pressure is defined by the condition of having Cerenkov light produced at angles $\theta \geq \theta^*$

$$P_{min} = \frac{T}{k} (n - 1)_{min} \tag{B5}$$

where $$(n - 1)_{min} = \frac{1}{\cos \theta^*} - 1 \tag{B6}$$

is the minimum value ($\rho = \infty$) for the gas refractive index.

The relations (B3), (B4) and (B5) are evaluated in the CEDAR control programmes taking into account the actual average gas temperature T .

2. Limits on mass definition from measuremen errors on P and T

From (B4) :

$$\Delta m = \Delta P^* \left(\frac{\partial m}{\partial P}\right) + \Delta T^* \left(\frac{\partial m}{\partial T}\right)$$

where ΔP^* and ΔT^* are the measurement errors on the gas parameters P and T .

Derivation of (B4) gives

$$\frac{\partial m}{\partial T} = - \frac{P}{T} \left(\frac{\partial m}{\partial P}\right)$$

$$\frac{\partial m}{\partial P} = \frac{k \cos \theta^*}{T} \left(\frac{p^2}{m}\right) \sqrt{1 + (m/p)^2} \simeq \frac{k \cos \theta^*}{T} \left(\frac{p^2}{m}\right) \tag{B7}$$

The mass uncertainty is then

$$\Delta m \simeq \frac{kP}{T} \frac{p^2}{m} \cos \theta^* \left(\frac{\Delta P^*}{P} + \frac{\Delta T^*}{T}\right) \tag{B8}$$

The functions (B7) and (B8) are plotted vs particle momentum in Figs

3. Some numerical evaluations of the above defined quantities are collected in the following table, assuming

$$T = 293.16\ K\ (20^{o}C)$$
$$\lambda = 300\ nm.$$

CEDAR type	$\dot{W}$	N	
gas	N_2	He	
k	8.44665×10^{-2}	9.59168×10^{-3}	K/bar (+)
Θ	30.9	25.8	mrad
P_{min}	1.647	10.175	bar
P_{max}	8	15	bar
$(n - 1)_{min}$	4.745×10^{-4}	3.329×10^{-4}	
ΔP	1.6	3	mbar } requested accuracies (++)
ΔT	0.3	0.1	K } requested accuracies (++)
ΔP^*	$\pm$ 0.5	$\pm$ 1	mbar } instrumental errors
ΔT^*	$\pm$ 0.02	$\pm$ 0.02	K } instrumental errors
$\left(\Delta P^* + P_{max} \frac{\Delta T^*}{T}\right)_{max}$	$\leq \pm$ 1	$\leq \pm$ 2	mbar

(+) Ref. 7)

(++) As from Table IV.

FIGURE CAPTIONS

Fig. 1 CEDAR counters installed in a secondary beam lines

Fig. 2 Schematics of the optics of a differential Cerenkov counter

Fig. 3 Velocity difference $\Delta\beta/\beta$ vs momentum for various pairs of particles with masses m_1 and m_2

Fig. 4 Photon distribution in the plane of the diaphragm (the shaded areas represent the diaphragm opening)

a) Good alignment

b) Broadening of the light spot due to multiple scattering incurred by the particle along the radiator

c) Missalignment

d) Effect of the beam divergence

Fig. 5 CEDAR efficiency as a function of beam divergence

Fig. 6 Multiple scattering for CEDAR West (gas : N_2)

Fig. 7 Multiple scattering for CEDAR North (gas : He)

Fig. 8 Efficiency as a function of the average number of photo-electrons per photomultiplier.

Fig. 9 Chromatic corrector optics

a) Corrector of DISC optics (ref. 1)

b) Corrector with two quartz lenses

Fig. 10 a) CEDAR optical elements enlarged to show their real shape and located in a distorted drawing of the optical trajectories.

b) CEDAR optics on real scale

Fig. 11 CEDAR resolution. For both CEDAR-W and CEDAR-N the chromaticity ΔR_{ch}, and its remanent value after correction ΔR_{cor}, are compared to the separation between pions and kaons $\Delta R_{k,\pi}$ and the effect of the multiple scattering undergone by the beam ΔR_{ms}.

Fig. 12 Scatter fringe interferogram taken at the functional focus of the Mangin mirror.

Fig. 13 Diagramme of light path for optical test of the assembled system.

Fig. 14 Effective radiator length for a hollow mirror

Fig. 15 Photon distribution on the mirror from a particle belonging to the edge of the beam.

Fig. 16 Light production, transmission and detection versus photon wave length.

Fig. 17 Photograph of the light diaphragme where two of the eight sectors can be seen.

Fig. 18 Typical layout of two CEDAR counters and associated equipment in a beam line (H6).

Fig. 19 Block diagram of CEDAR electronics

Fig. 20,21 Radial distance in the plane of the diaphragme between the light rings of the wanted and of various unwanted particles, versus beam momentum. The dotted line indicates the width of the light spot (4σ) and the dashed line gives the contribution to the light spot of the multiple scattering (4σ).

Fig. 20 : CEDAR-W, Fig. 21 : CEDAR-N

Fig. 22,23 CEDAR-N pressure scan showing the π/k separation in the H6 beam running at -175 GeV/c for two LD settings :

Fig. 22, LD = 0.50 mm

Fig. 23, LD = 0.71 mm

Fig. 24 LD scan with pressure set on the kaon mass. CEDAR-N in beam H6 as for Figs 22 and 23.

Fig. 25 Pressure scan for CEDAR-N showing the separation of electrons and pions at -60 GeV/c.

Fig. 26 Pressure scan for CEDAR-N showing the separation of electrons, muons and pions at +20 GeV/c.

Fig. 27 General mechanical drawing.

REFERENCES

1. M. Benot, J. Litt and R. Meunier,
Cerenkov counters for Particle Identification at High Energies,
N.I.M. 105 (1972), 431-444.

2. C. Bovet, S. Milner, A. Placci,
CERN/Lab. II/EA/74-4.

3. C. Bovet, R. Maleyran, A. Placci, M. Placidi,
The CEDAR (Cerenkov Differential Counters with Achromatic Ring focus) project - IEEE Nucl. Sc. Symp. 1978, vo. NS25, no.1, p. 512.

4. V.P. Zrelov,
Cerenkov Radiation in High-Energy Physics
Atomizdat Moskva 1968, translated from Russian by Israel Programme for Scientific Translations, Jerusalem 1970, Vol. I + Vol. II.

5. R. Feynmann,
Lectures of Physics, 31-8.

6. The Hamilton Standard MOdel 1D Digital Pressure Transducer
(Instruction Manual).

7. M. Placidi, SPS/EA/Note 76-20,
M. Placidi, SPS/EA/Note 76-21.

8. P. Dreesen, SPS/EBS/Note 78-15 (Rev. 2.4.1979).

9. C. Bovet, A. Placci, M. Placidi,
Paper in preparation.

10. H.W. Atherton, C. Bovet, N. Doble, G. Von Holtey, L. Piemontèse, A. Placci, M. Placidi, D.E. Plane, M. Reinharz and E. Rossa.
Precise measurements of particle production by 400 GeV/c protons on Beryllium targets.
CERN 80-07.

ACKNOWLEDGEMENTS

It is a pleasure to express our appreciation to S. Milner for leading the mechanical design effort at the beginning of the CEDAR project and to M. Rabany and members of his group for their design of the electronics and subsequent care in its implementation and operation. E. Rossa participated in the first tests of the optical system and, with the help of G.P. Ferri, has been responsible for the functioning of the CEDAR counters since 1980. M. Glaser took the initiative to improve the software package described in Chapter 4. In addition, we are grateful to all our EA colleagues who have worked with great competence to develop and operate the CEDAR counters. Among the many experimental teams who have made use of the counters we particularly wish to acknowledge the participation of T. Ekelöf in the early stages of operation and the interest and help shown by members of experiment NA3 in exploiting CEDARs at high particle fluxes.

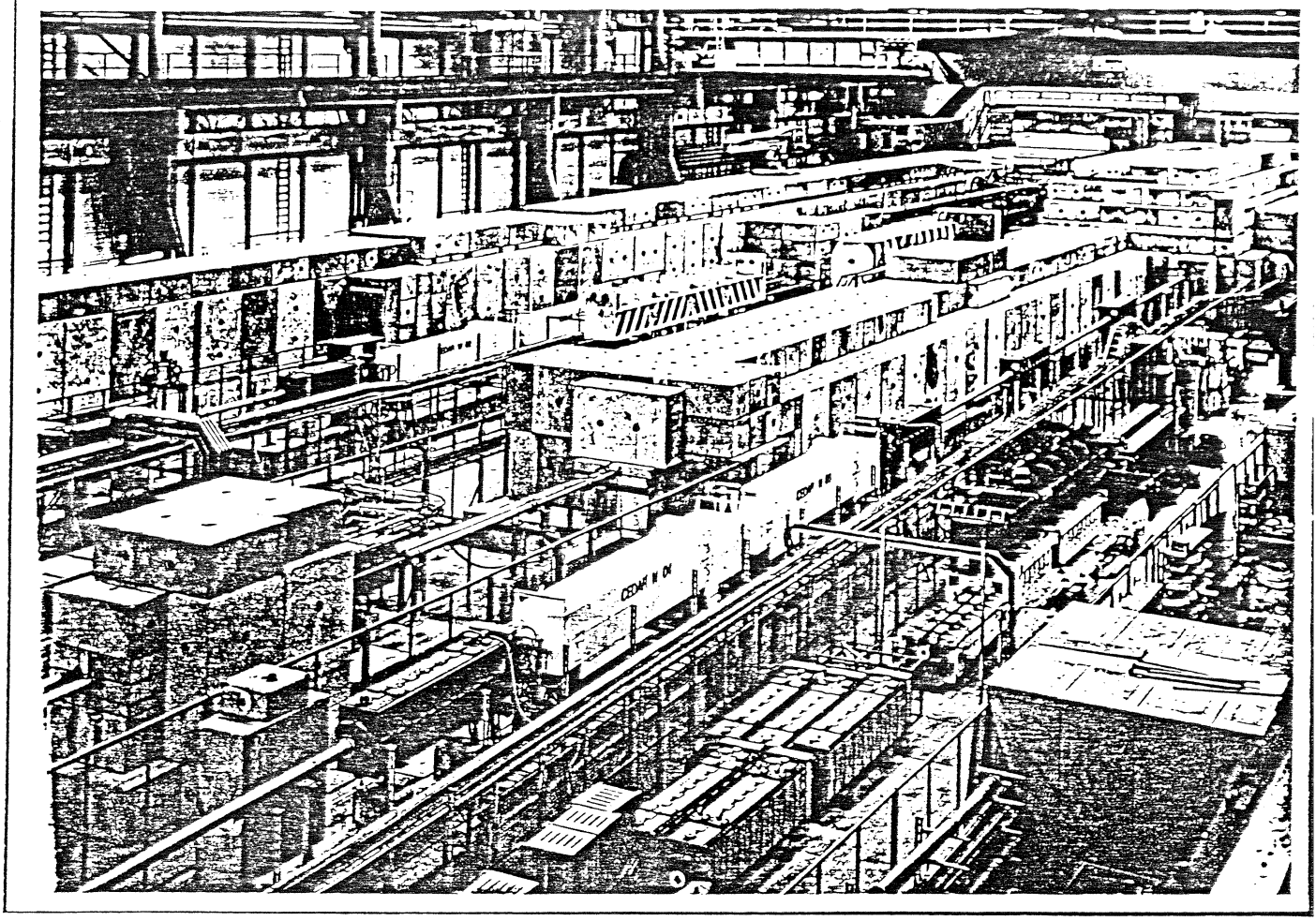

fig. 1

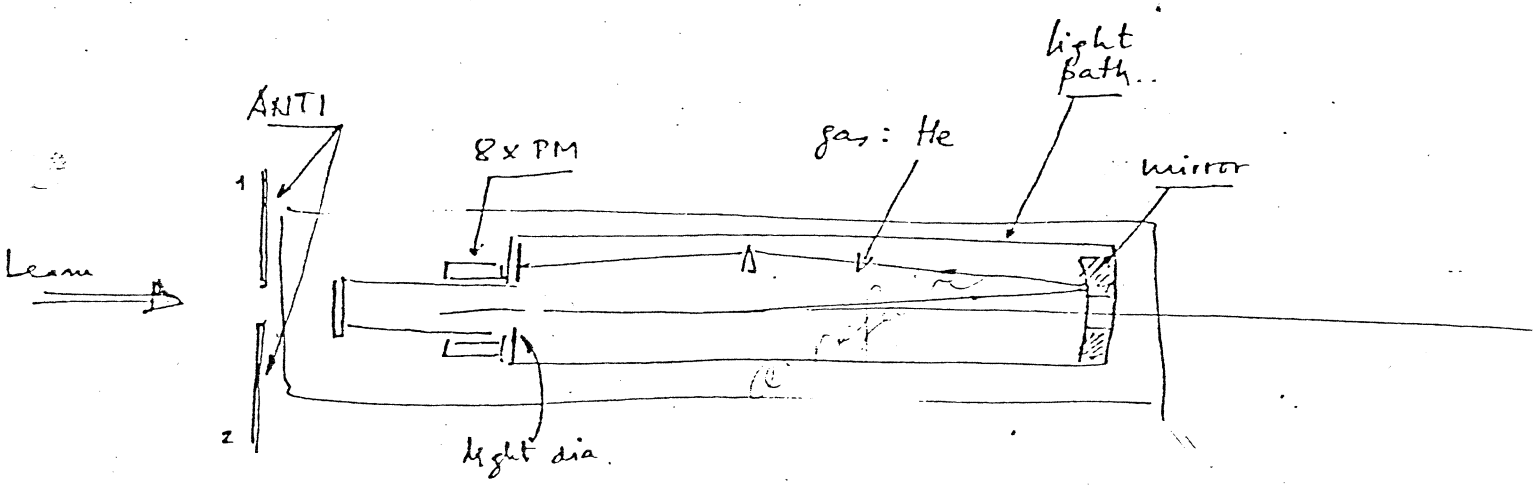

CEDAR SCHEMATICS

fig. 2

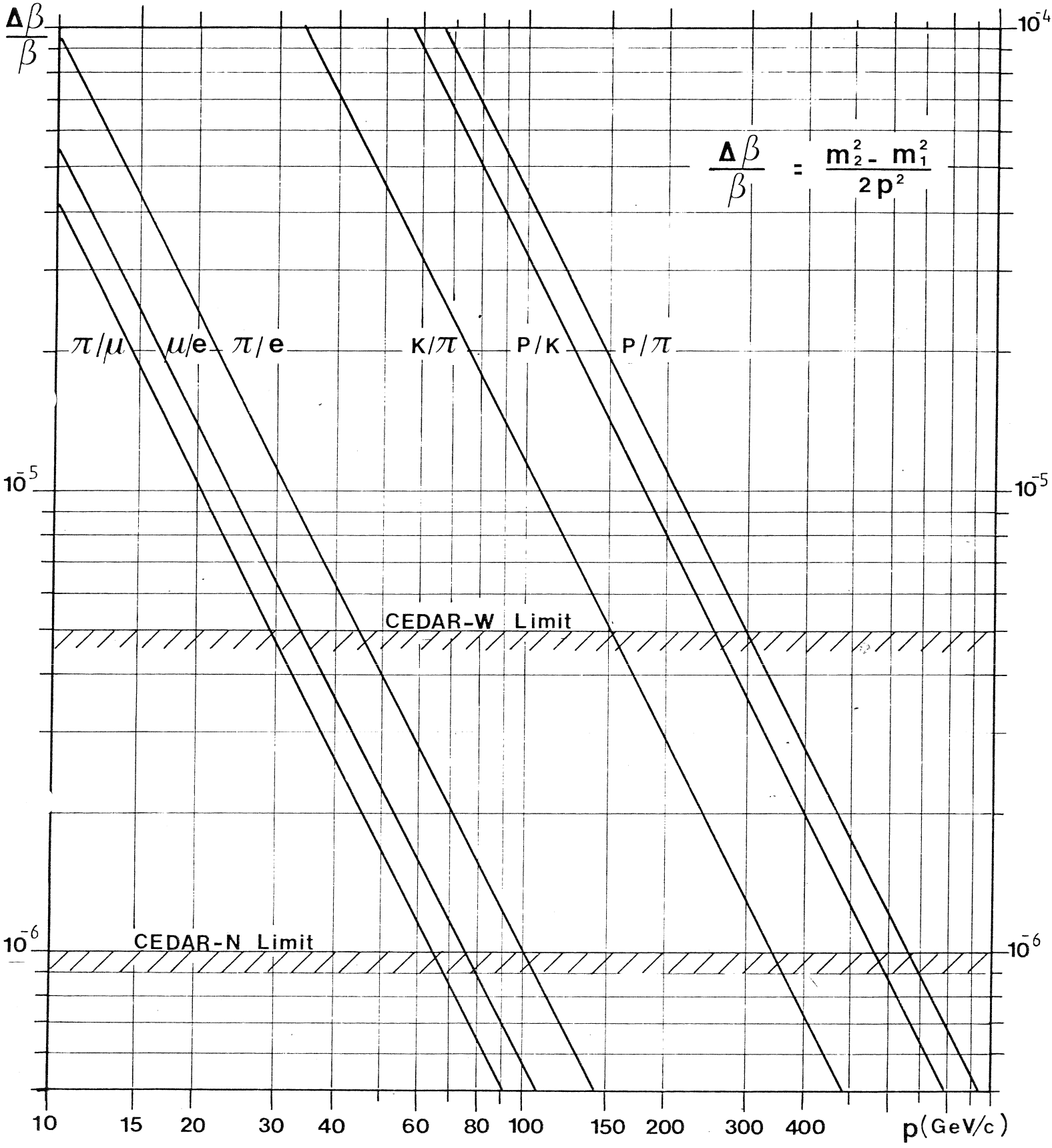
Δβ/β
$\frac{\Delta\beta}{\beta} = \frac{m_2^2 - m_1^2}{2p^2}$
π/μ
μ/e
π/e
K/π
P/K
P/π
CEDAR-W Limit
CEDAR-N Limit
10⁻⁴
10⁻⁵
10⁻⁶
10
15
20
30
40
60
80
100
150
200
300
400
p(GeV/c)

fig.3

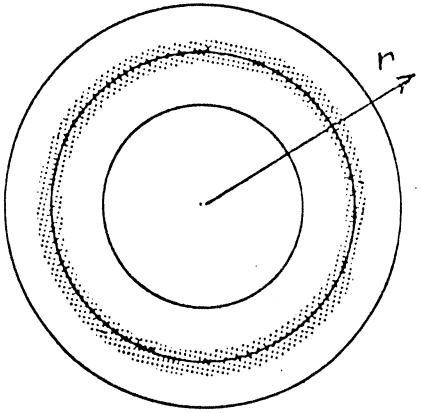

Good alignement

a

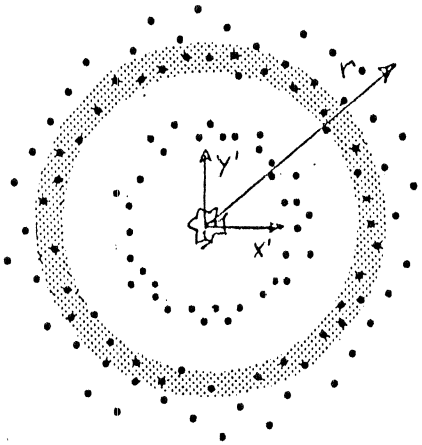

Multiple scattering

b

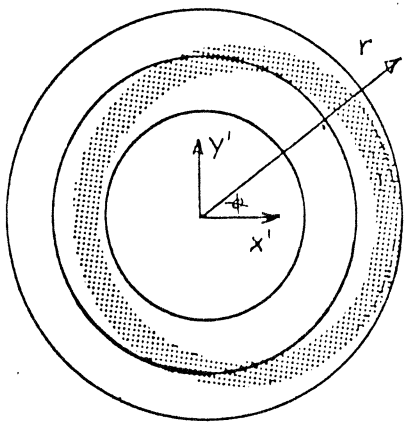

Misalignement

c

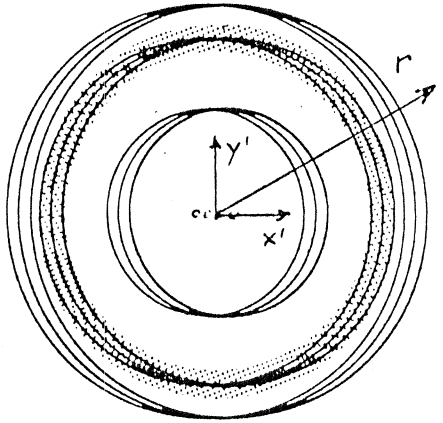

Beam divergence
(horizontal)

d

Fig 4.

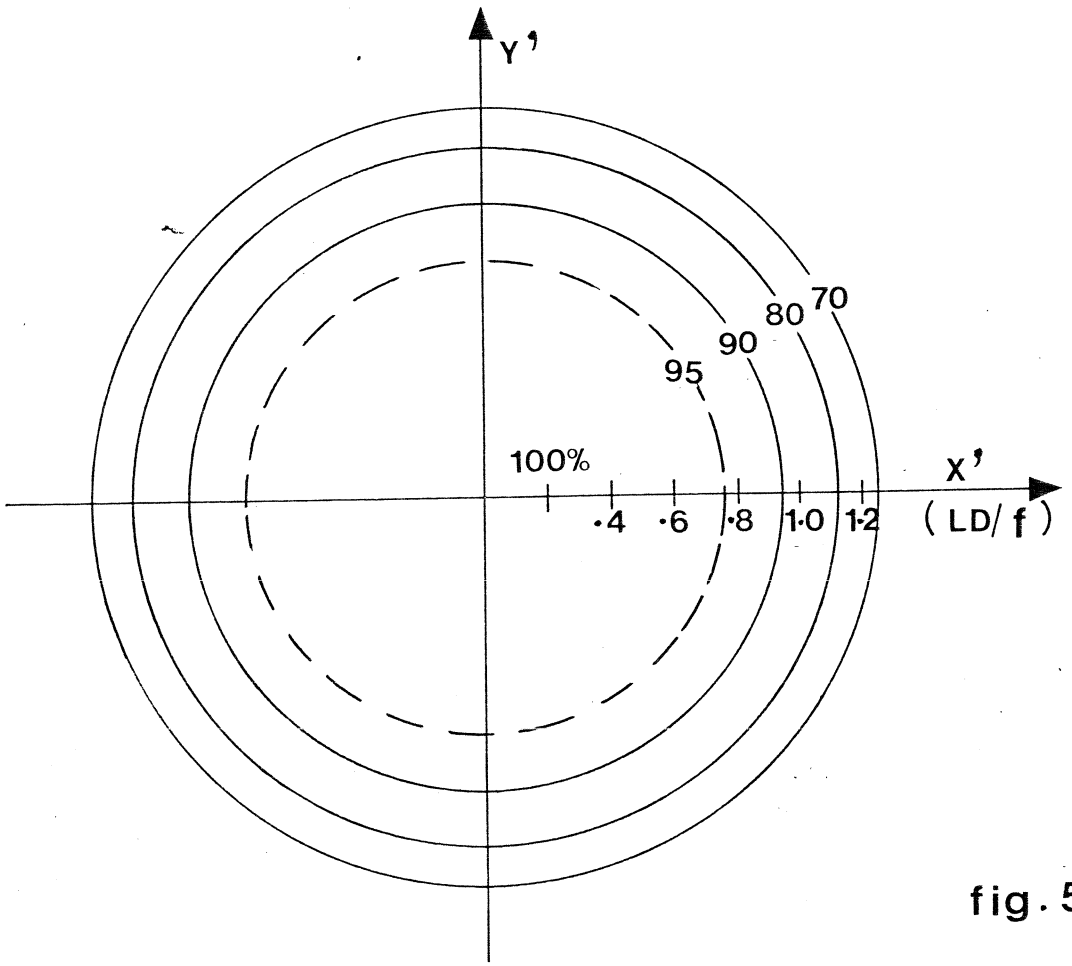

fig. 5

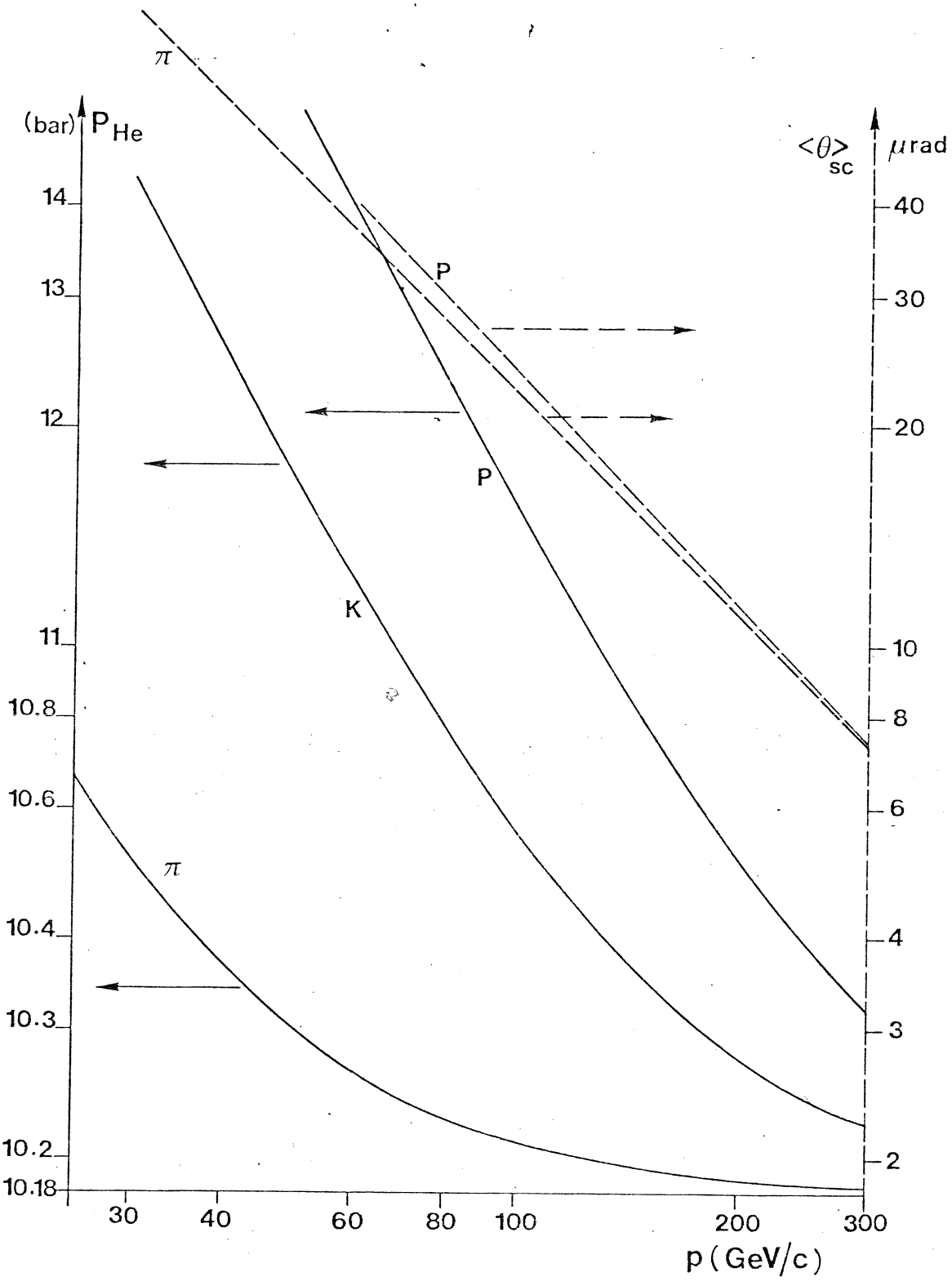
π
(bar) P He
14
13
12
11
10.8
10.6
10.4
10.3
10.2
10.18
P
P
K
π
<θ> sc
μrad
40
30
20
10
8
6
4
3
2
30
40
60
80
100
200
300
p (GeV/c)

fig.6

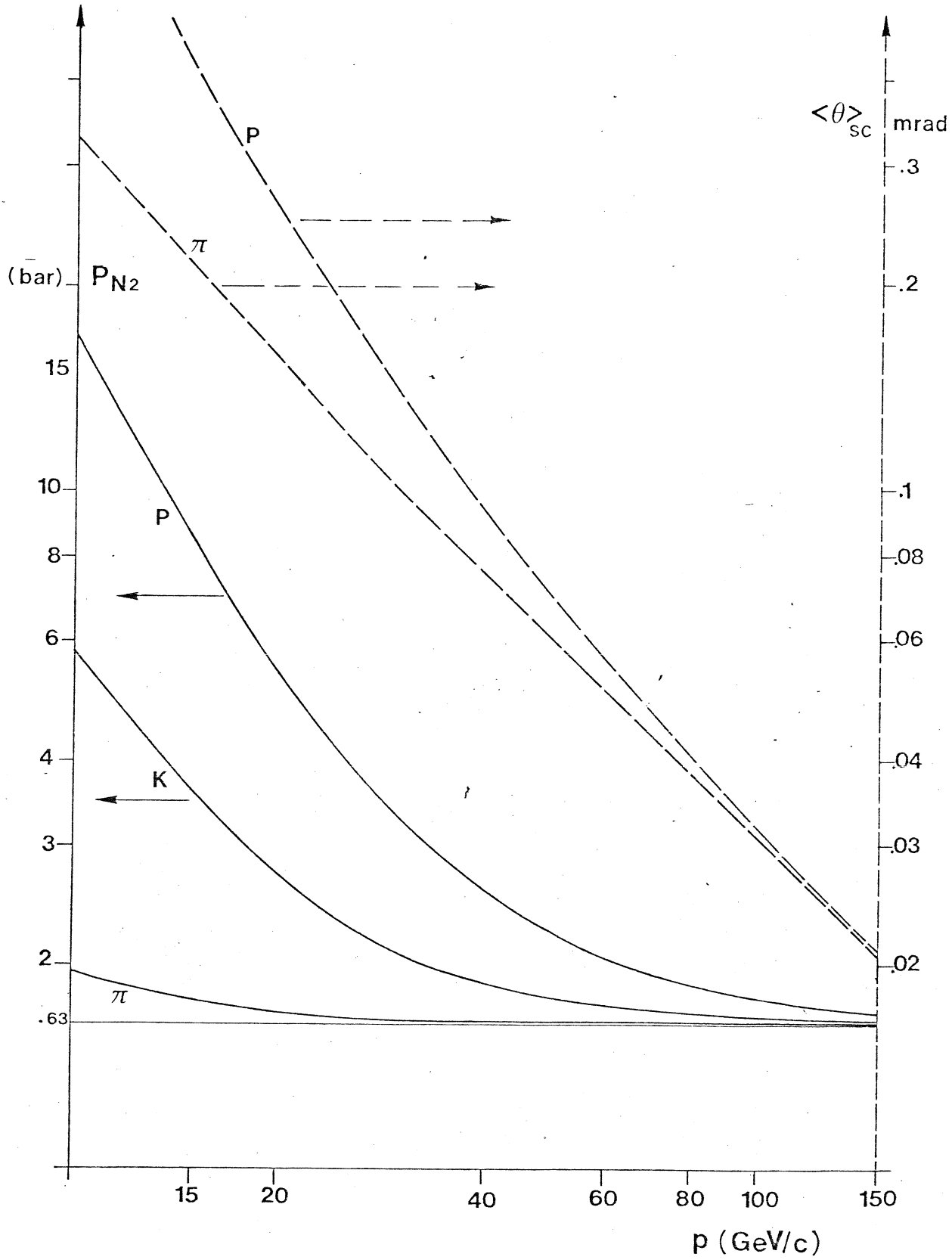
P
π
(bar) P_{N_2}
15
10
8
6
4
3
2
.63
P
K
π
$\langle\theta\rangle_{sc}$ mrad
.3
.2
.1
.08
.06
.04
.03
.02
15
20
40
60
80
100
150
p (GeV/c)

fig.7

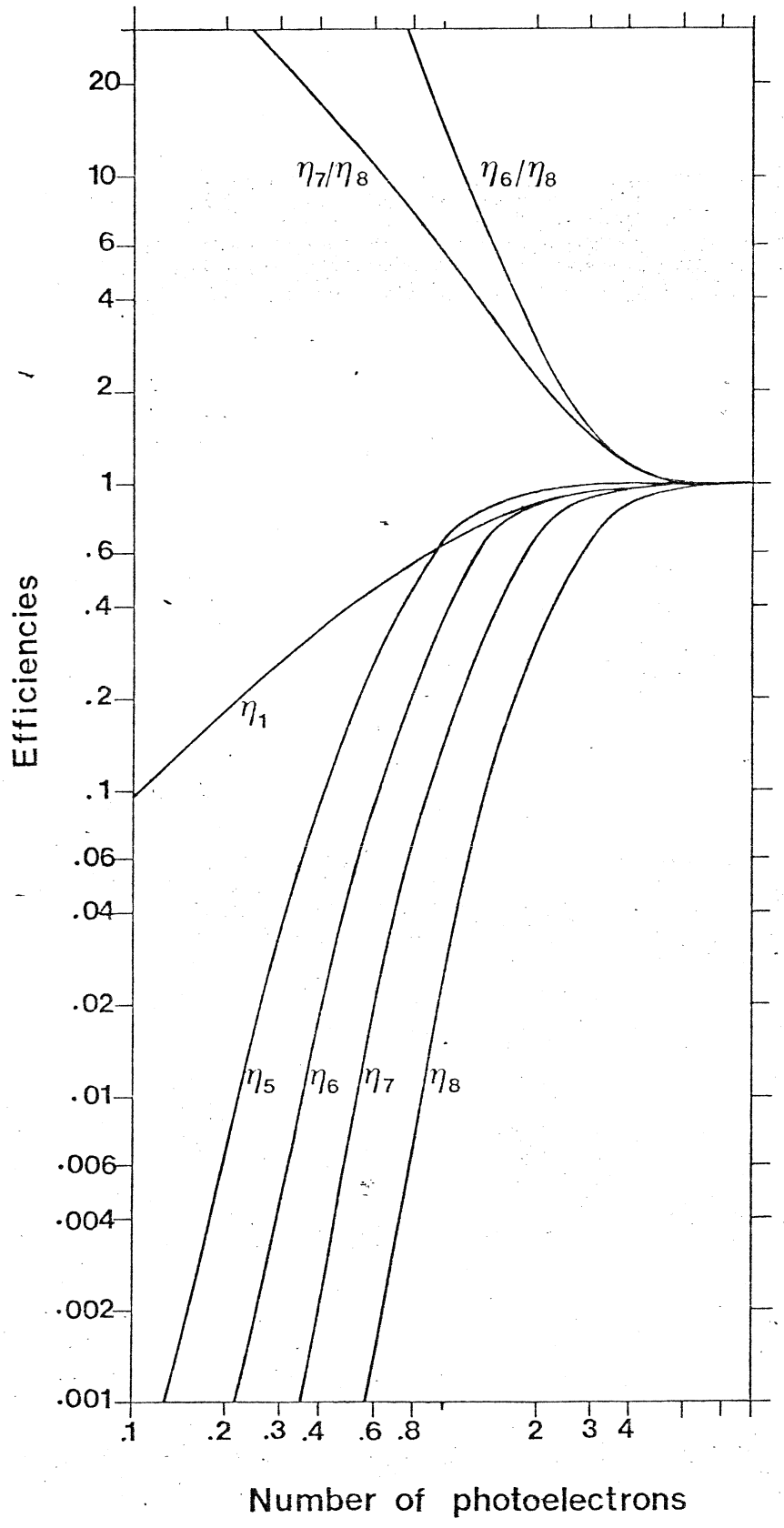
Efficiencies
20
10
6
4
2
1
.6
.4
.2
.1
.06
.04
.02
.01
.006
.004
.002
.001
η_7/η_8
η_6/η_8
η_1
η_5
η_6
η_7
η_8
.1
.2
.3
.4
.6
.8
2
3
4
Number of photoelectrons

fig.8

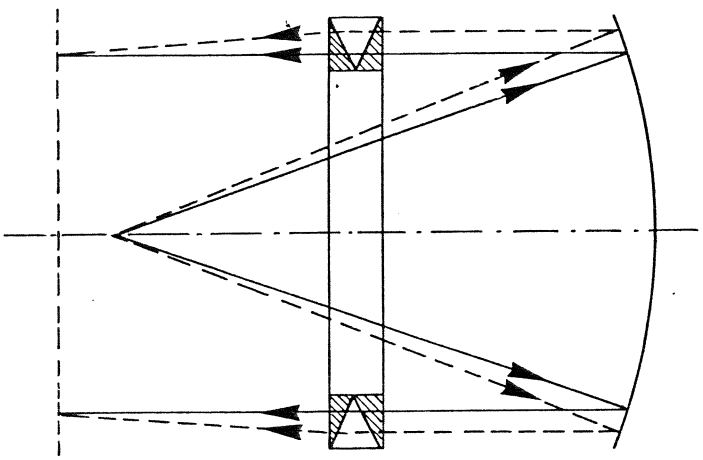

fig . 9a

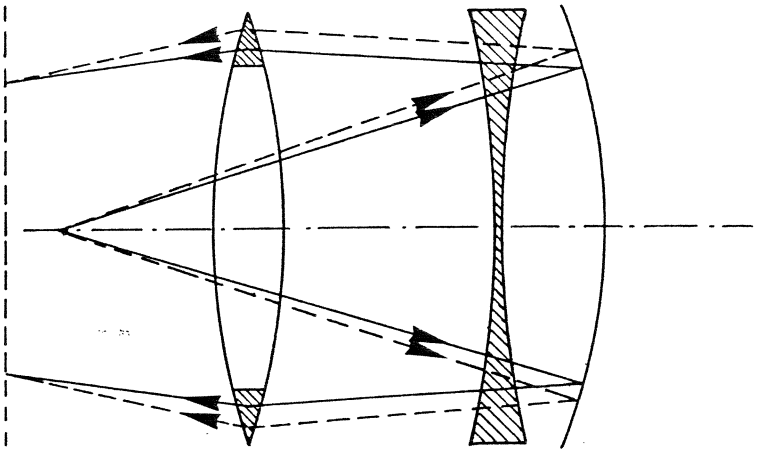

fig . 9b

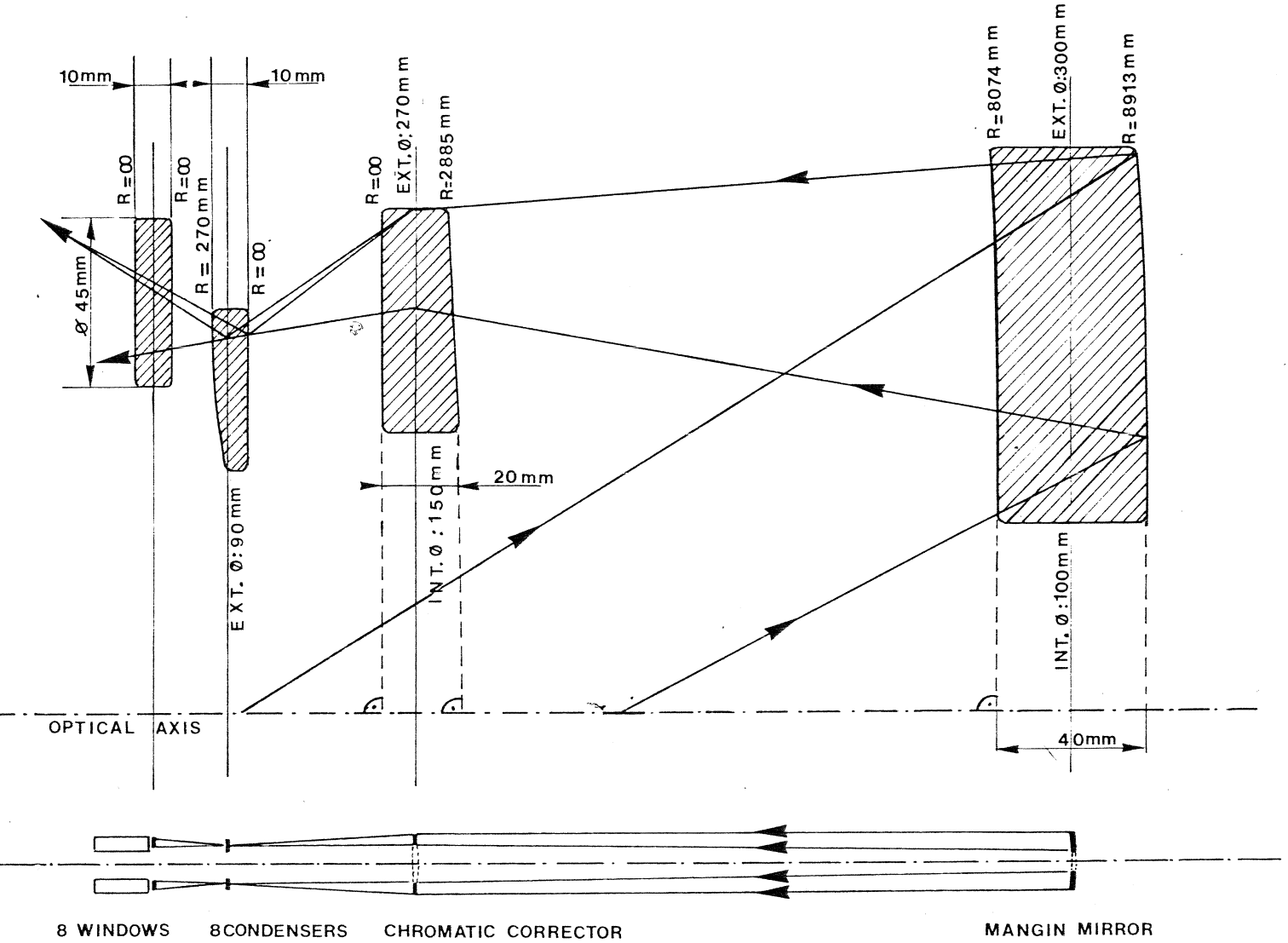

fig . 11

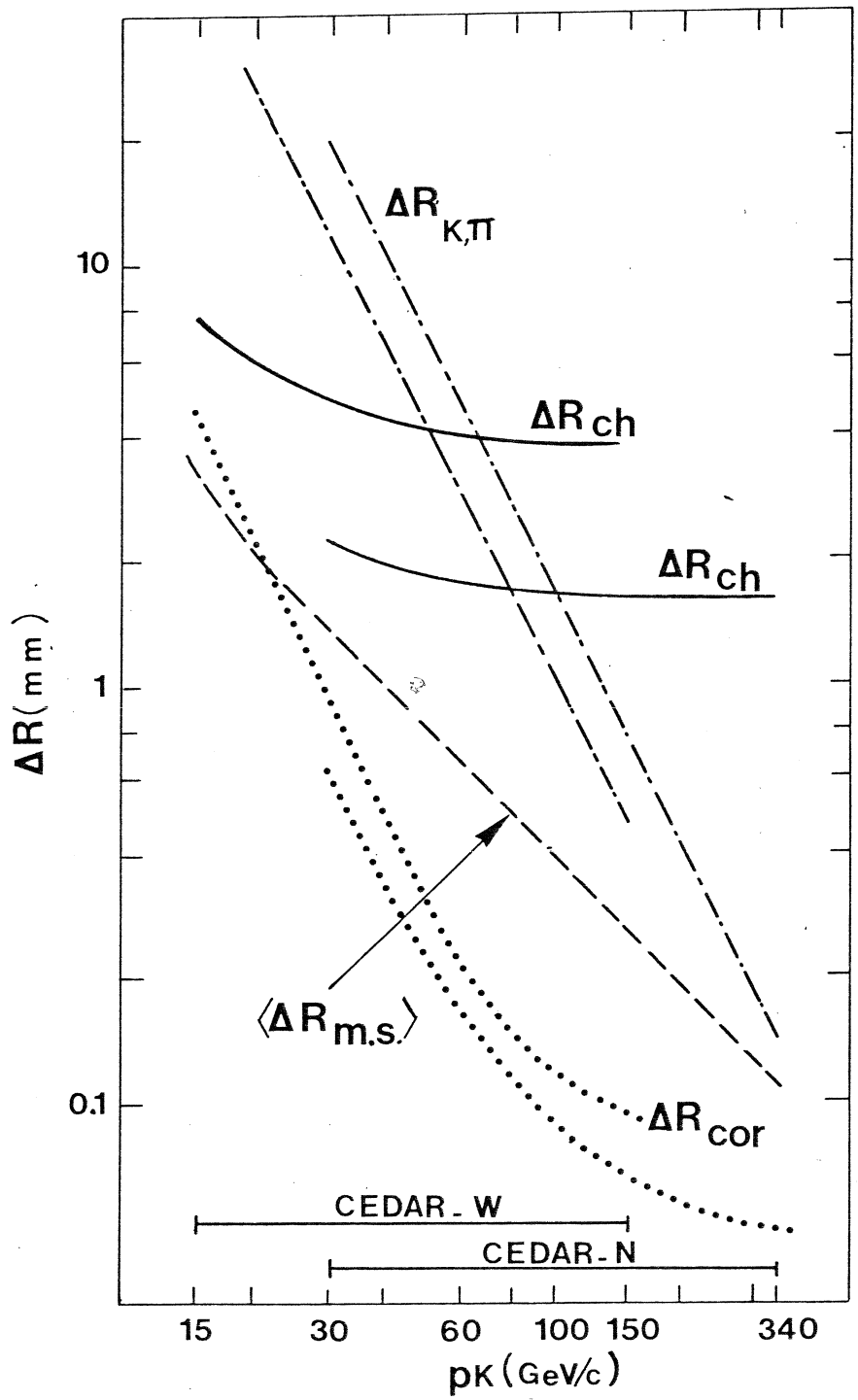
ΔR K,π
ΔR ch
ΔR ch
⟨ΔR m.s.⟩
ΔR cor
CEDAR - W
CEDAR - N
10
1
0.1
ΔR (mm)
15
30
60
100
150
340
pK (GeV/c)

fig.10

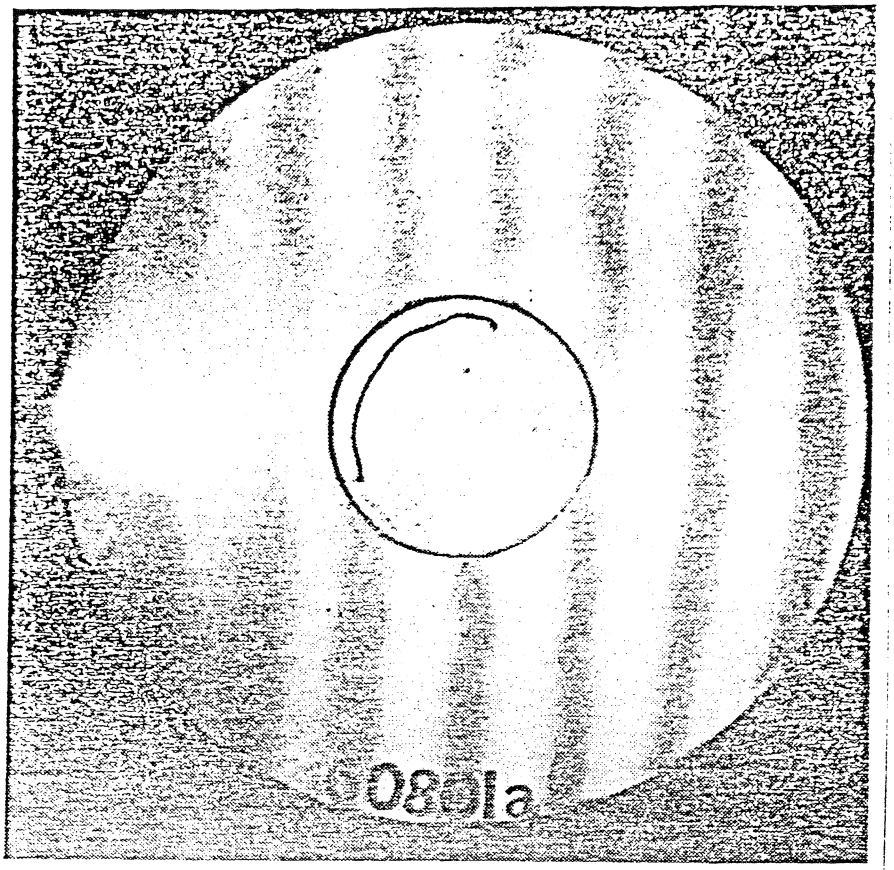

Fig.12.

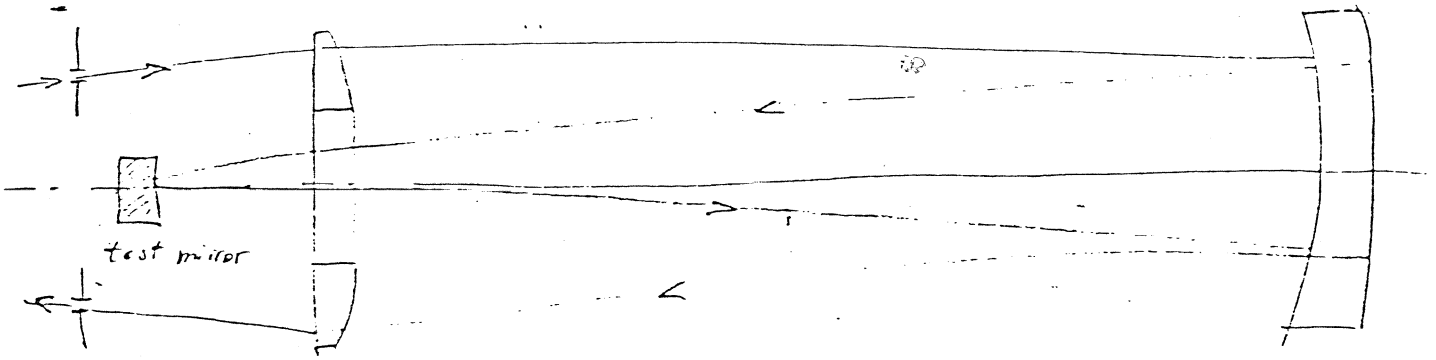

Fig.13

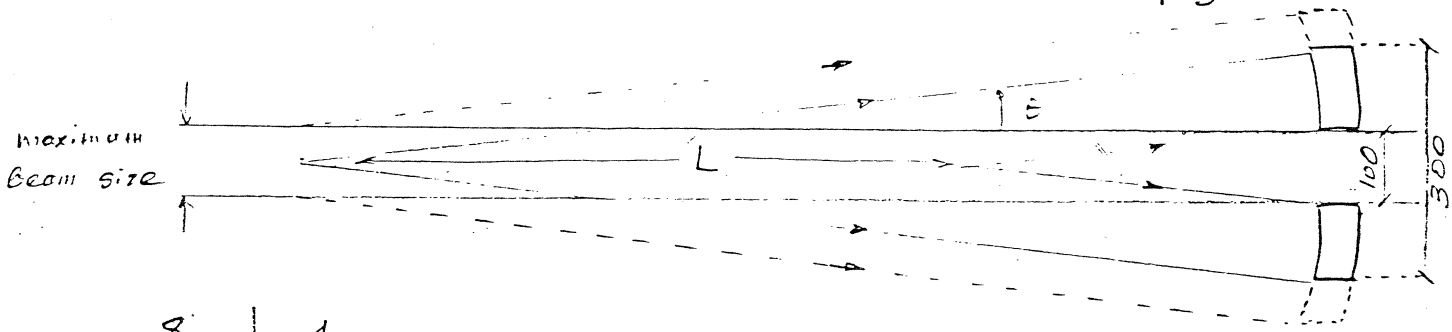

Fig 14

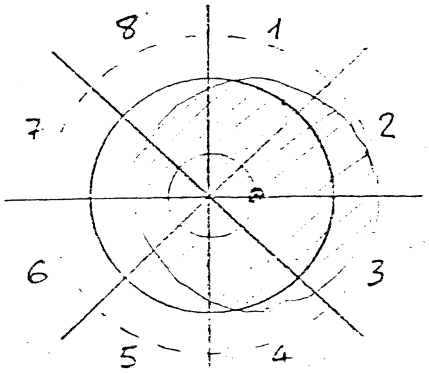

Fig.15

LIGHT PRODUCTION, TRANSMISSION and DETECTION

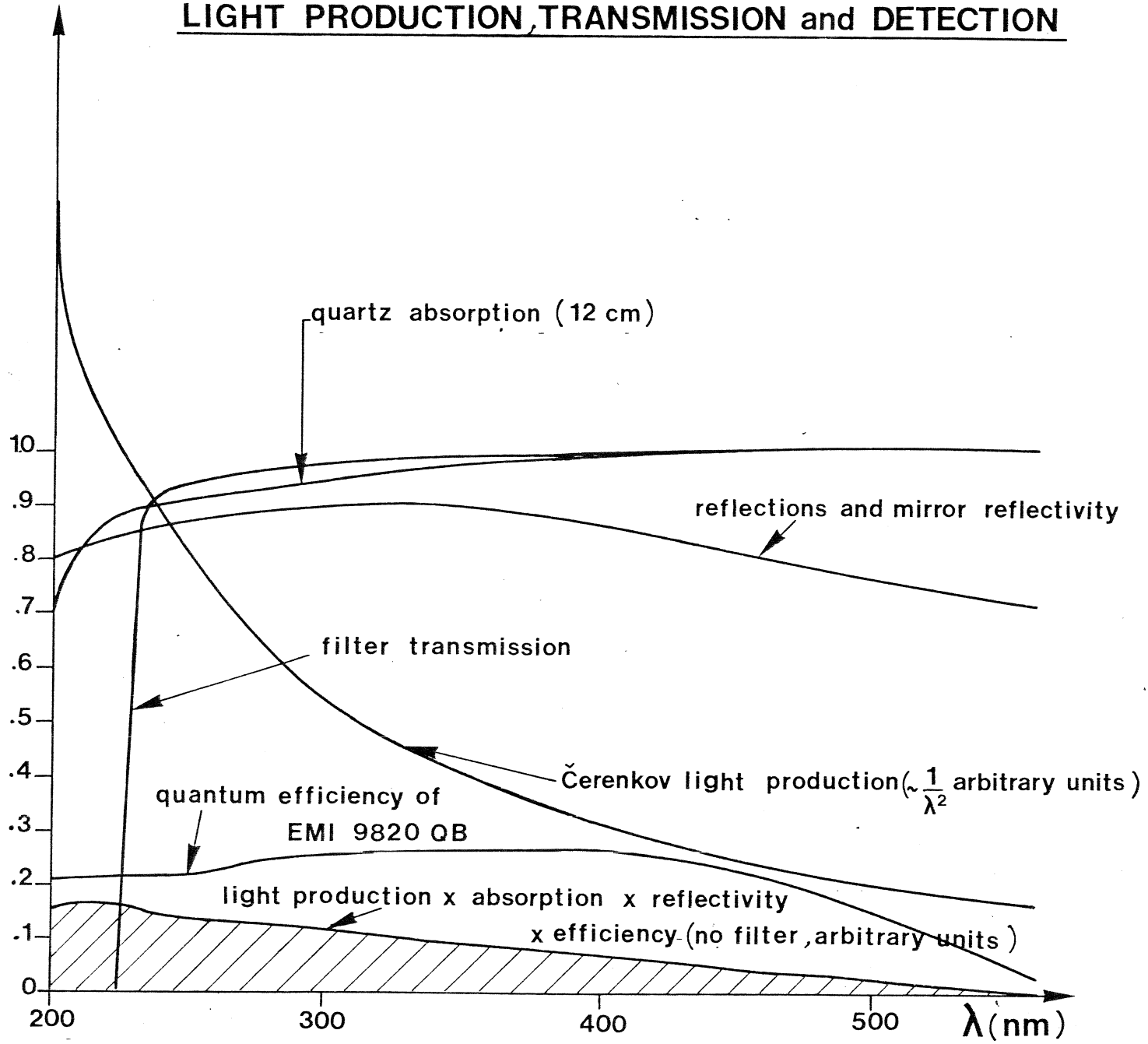

fig.16

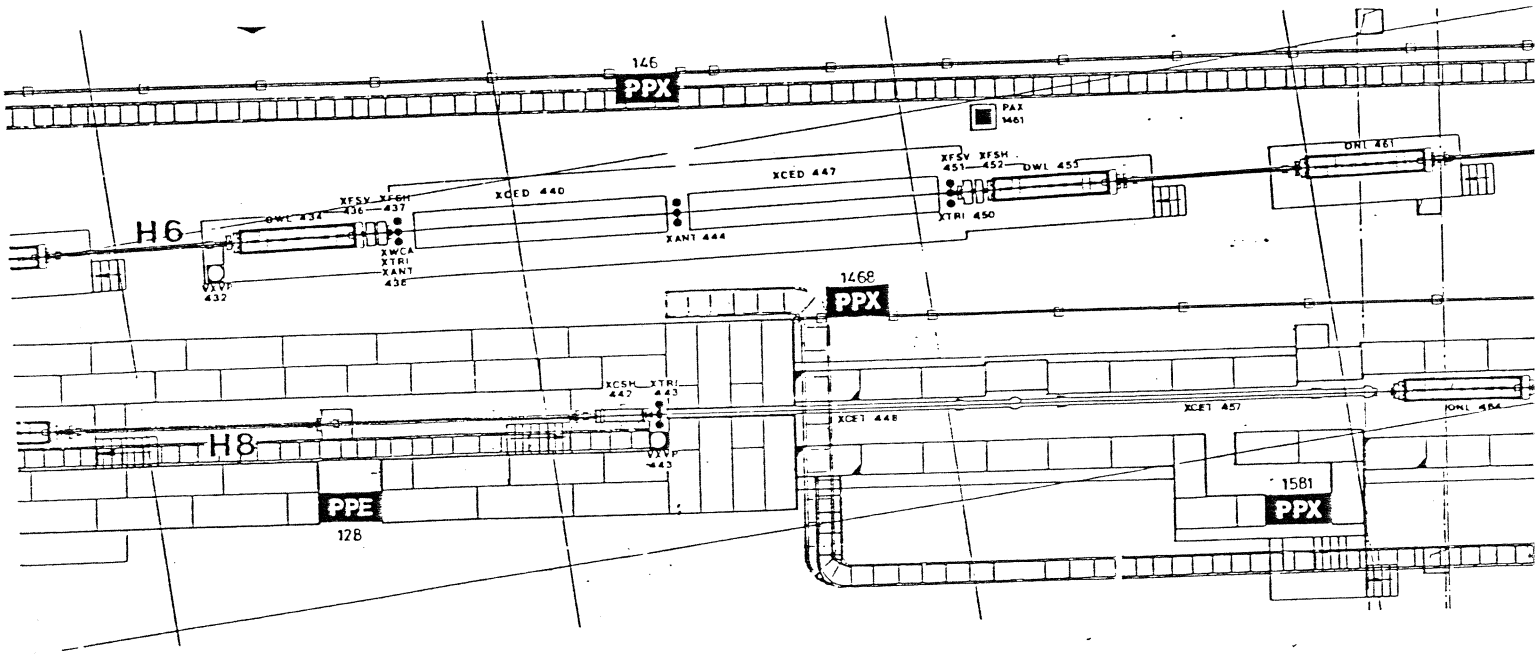
146
PPX
PAX
1461
XFSV XFSH
451 452
DWL 455
DNL 461
XCED 447
XCED 440
XFSV XFSH
436 437
DWL 434
H6
XTRI 450
XANT 444
XWCA
XTRI
XANT
436
VXVP
432
1468
PPX
XCSH XTRI
442 443
XCET 448
XCET 457
DNL 464
H8
VXVP
443
1581
PPX
PPE
128

Fig. 18

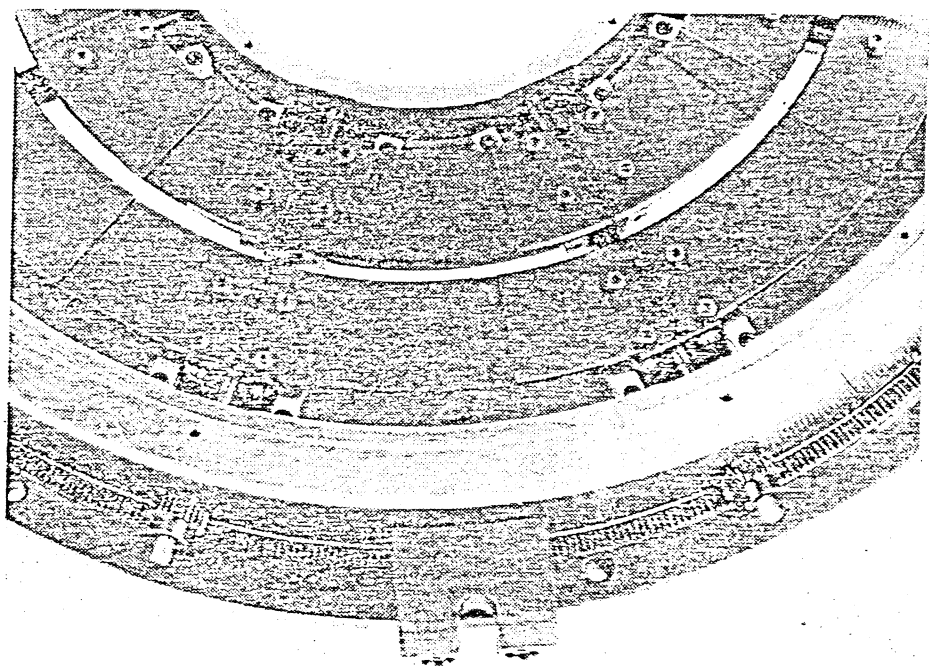

Fig. 17

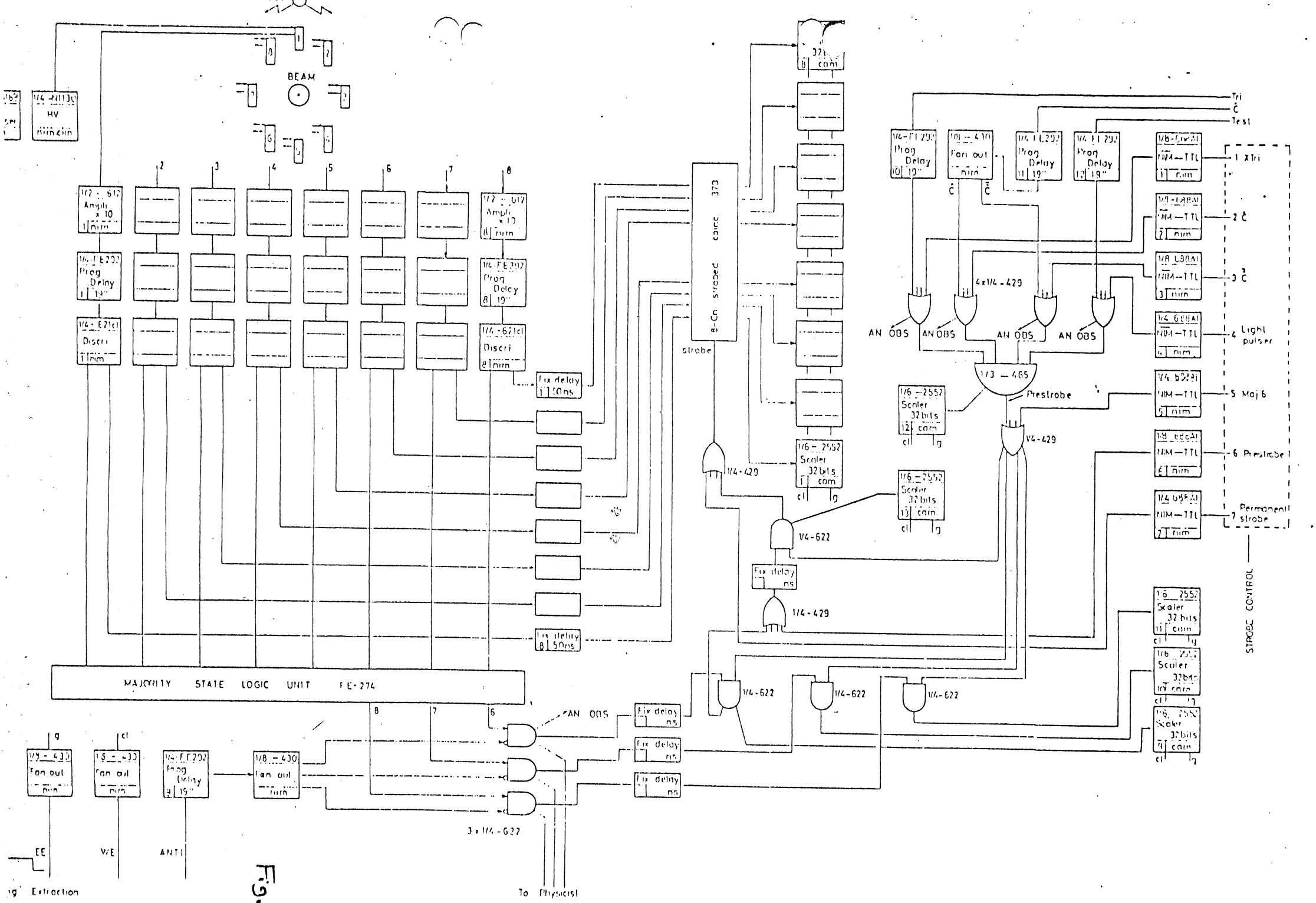
BEAM
MAJORITY STATE LOGIC UNIT FE-274
Prog Delay
Discri
Fix delay
Scaler 32 bits
Fan out
Prestrobe
Permanent strobe
STROBE CONTROL
To Physicist
EE
V/E
ANTI
Extraction
Extraction

Fig. 19

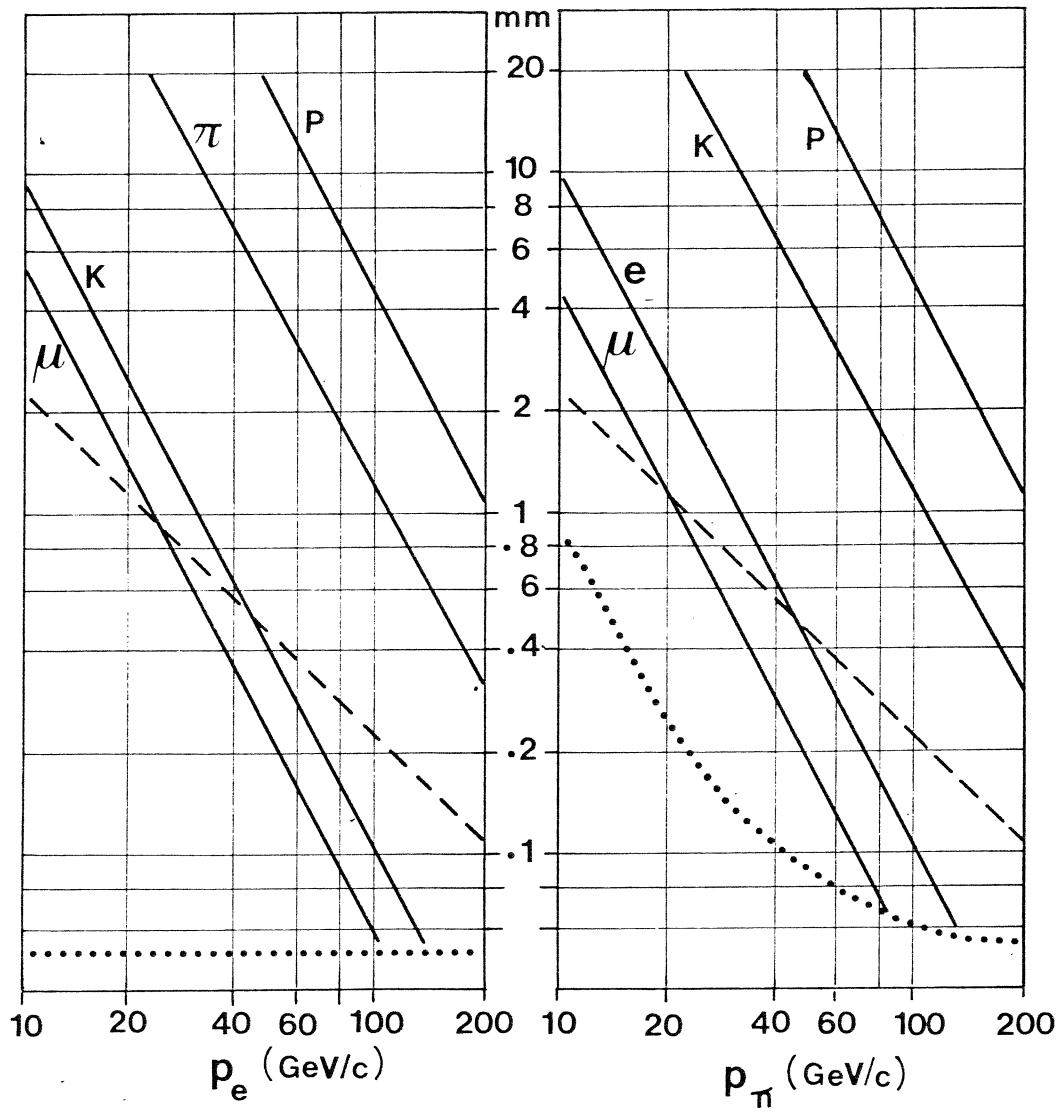
mm
20
10
8
6
4
2
1
.8
.6
.4
.2
.1
π
P
K
μ
e
10
20
40
60
100
200
p_e (GeV/c)
p_π (GeV/c)

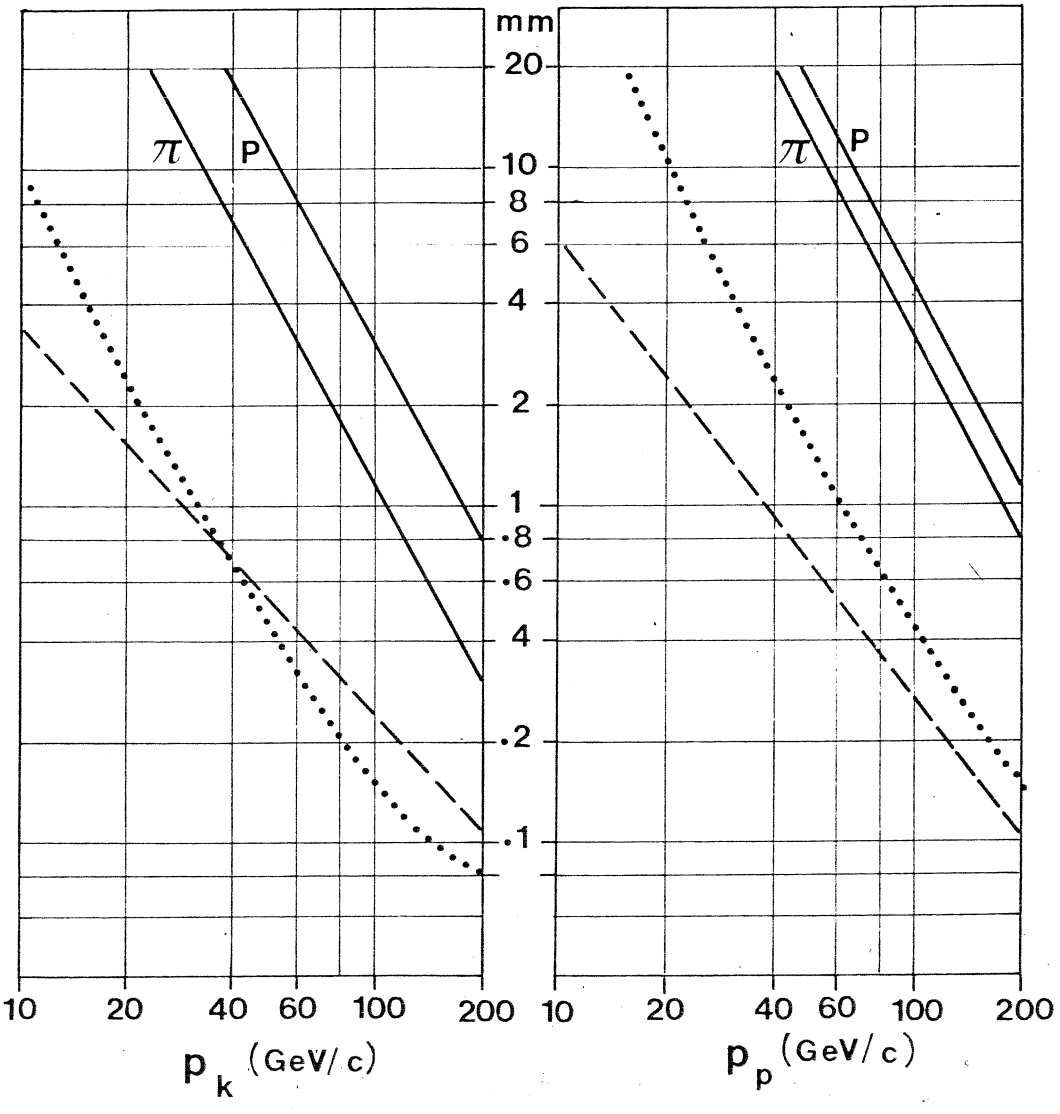
mm
20
10
8
6
4
2
1
.8
.6
.4
.2
.1
π
P
10
20
40
60
100
200
p_k (GeV/c)
p_p (GeV/c)

fig.20

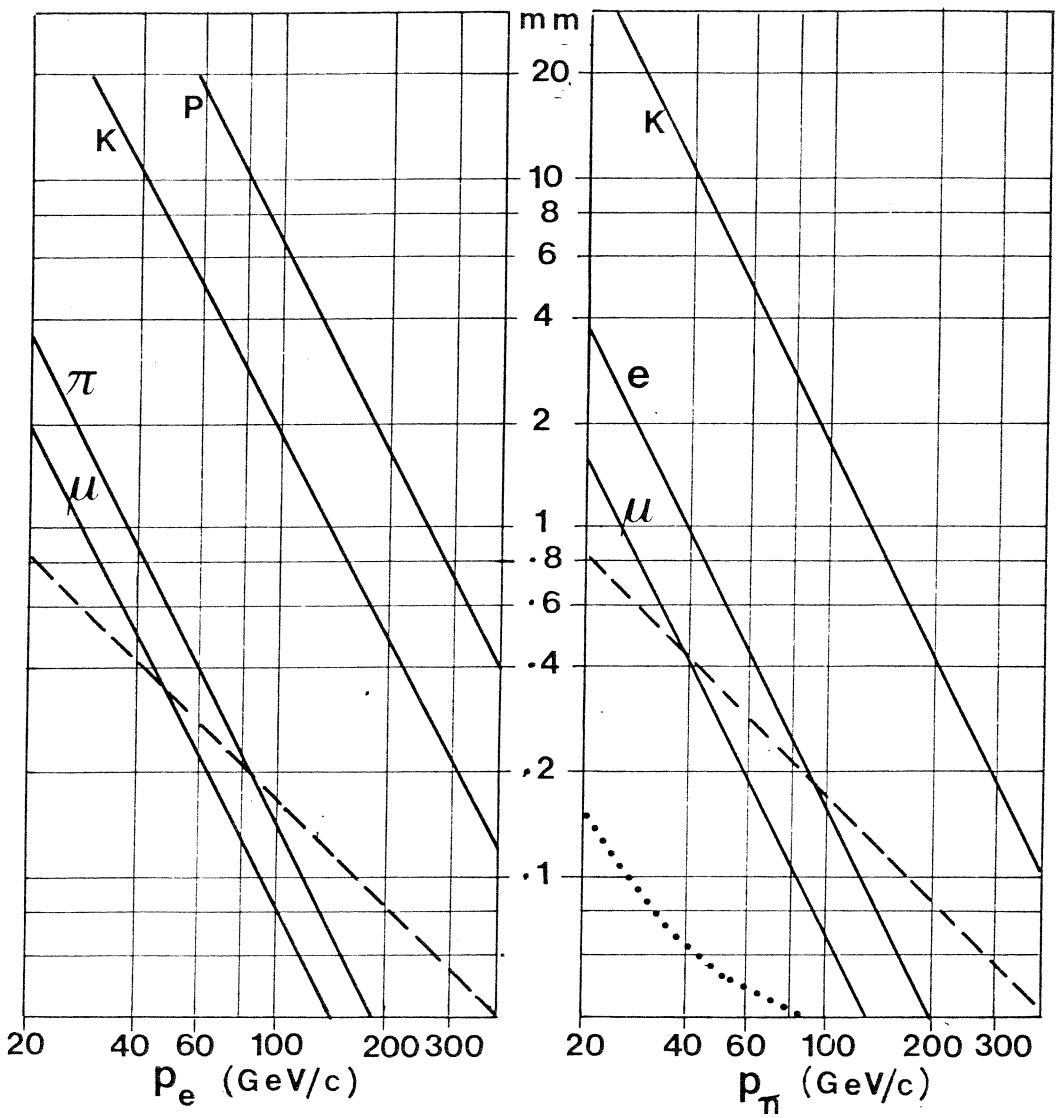
m m
20
10
8
6
4
2
1
·8
·6
·4
·2
·1
K
P
π
μ
20 40 60 100 200 300
p_e (GeV/c)
K
e
μ
20 40 60 100 200 300
p_π (GeV/c)

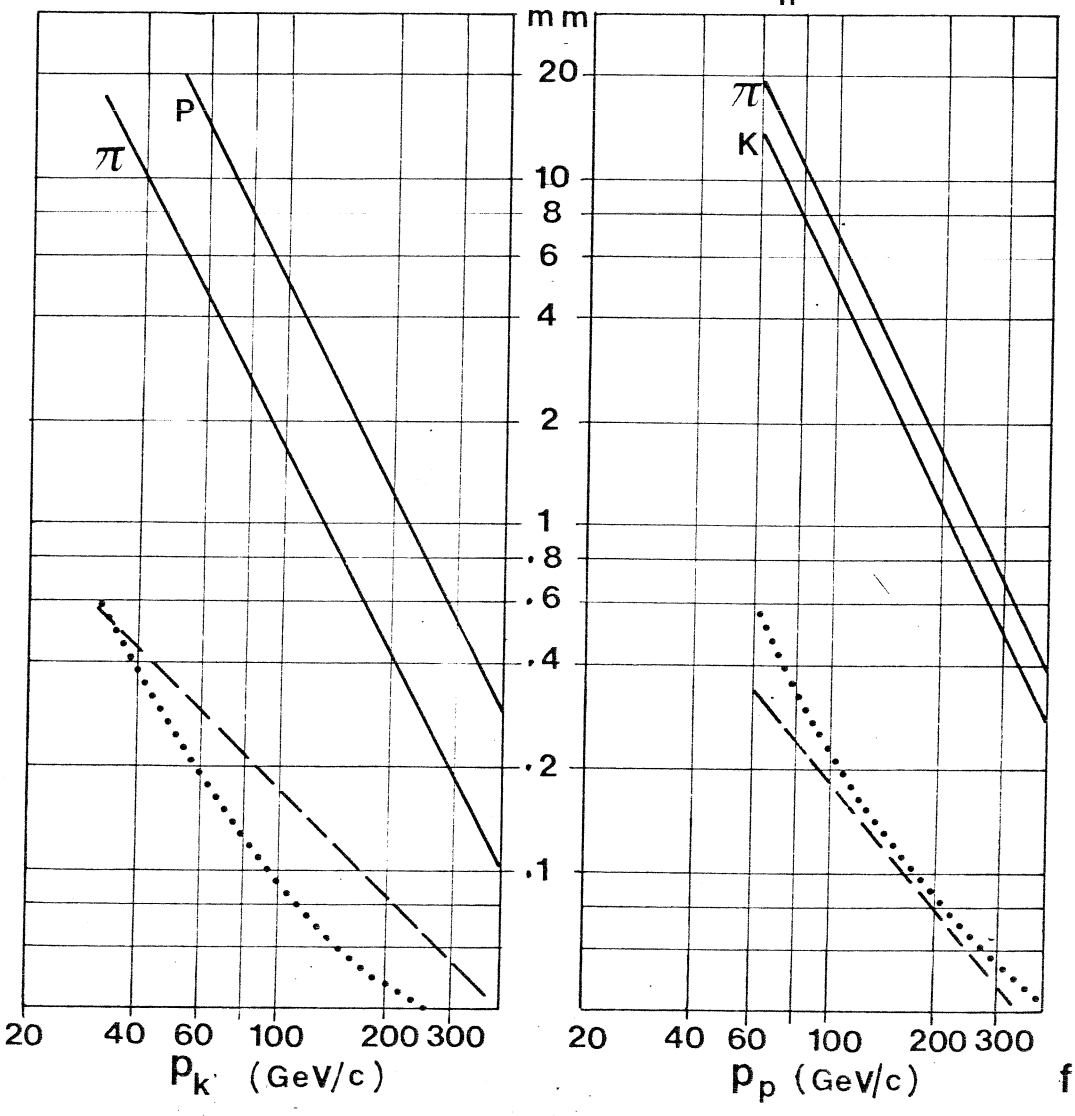
m m
20
10
8
6
4
2
1
·8
·6
·4
·2
·1
P
π
20 40 60 100 200 300
p_k (GeV/c)
π
K
20 40 60 100 200 300
p_p (GeV/c)

fig.21

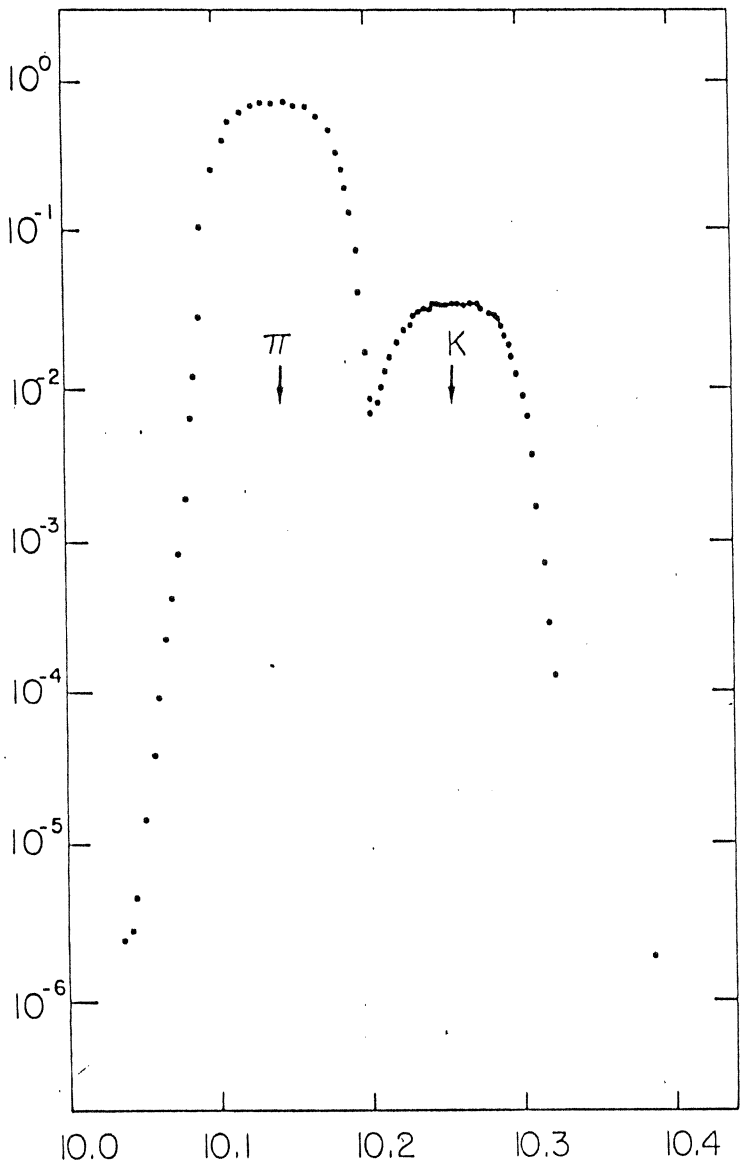
10^0
10^{-1}
10^{-2}
10^{-3}
10^{-4}
10^{-5}
10^{-6}
π
K
10.0
10.1
10.2
10.3
10.4
p (bar)

Fig. 22

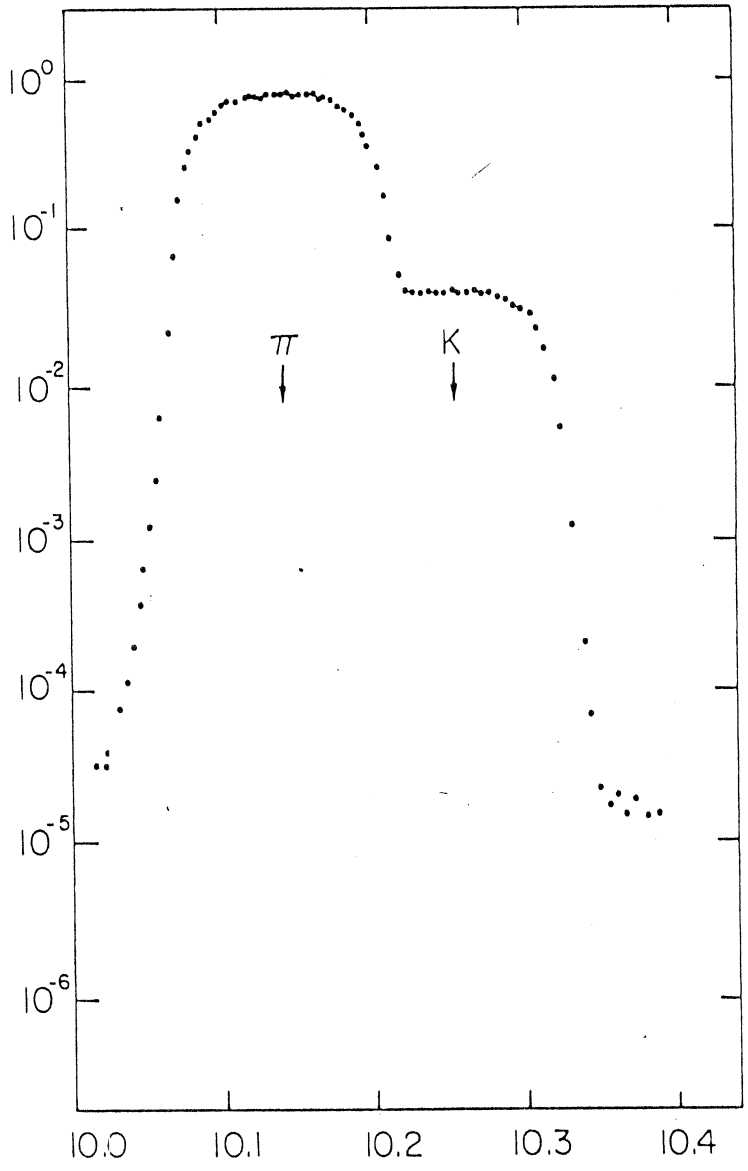
10^0
10^{-1}
10^{-2}
10^{-3}
10^{-4}
10^{-5}
10^{-6}
π
K
10.0
10.1
10.2
10.3
10.4
p (bar)

Fig. 23

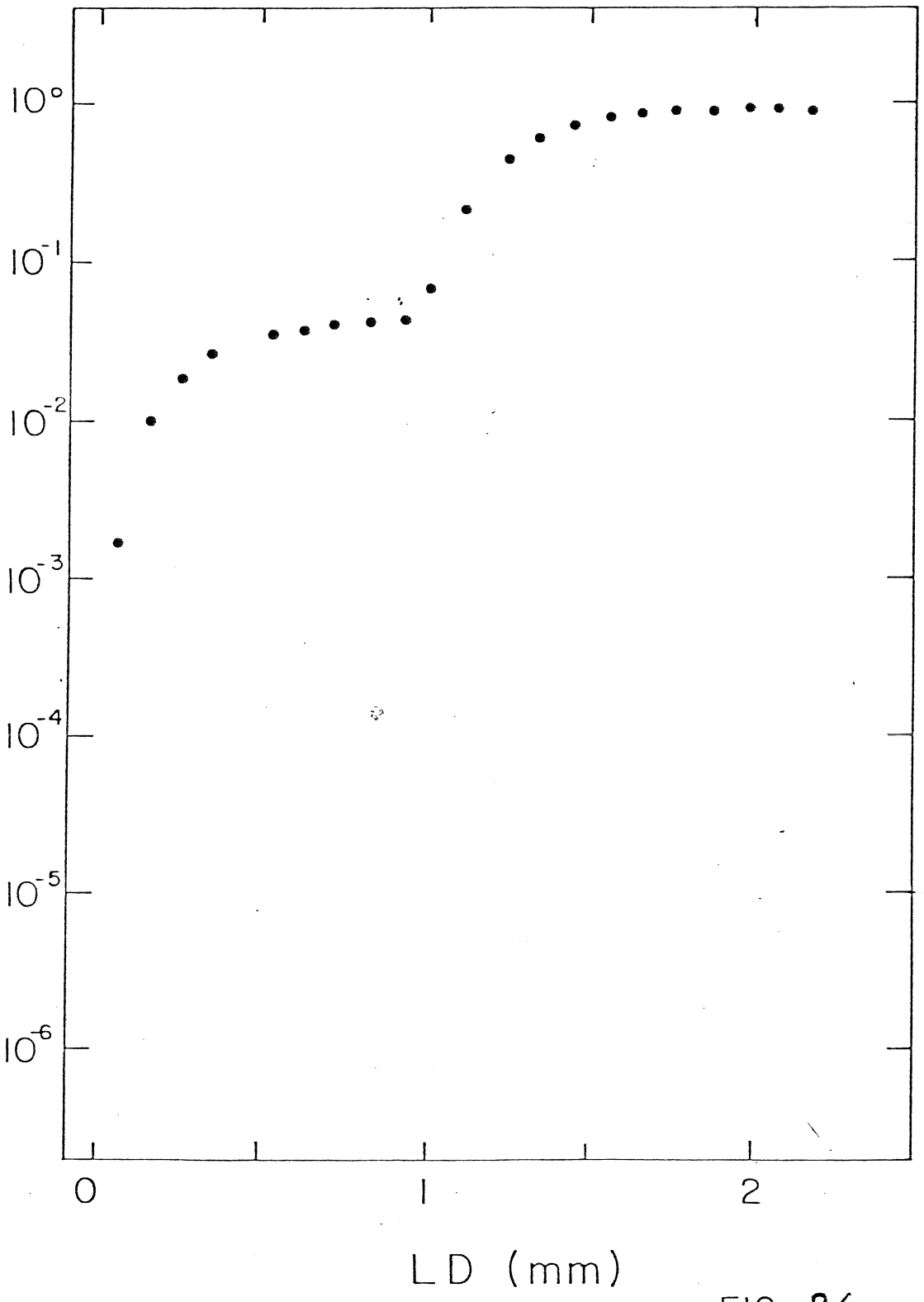

FIG. 24

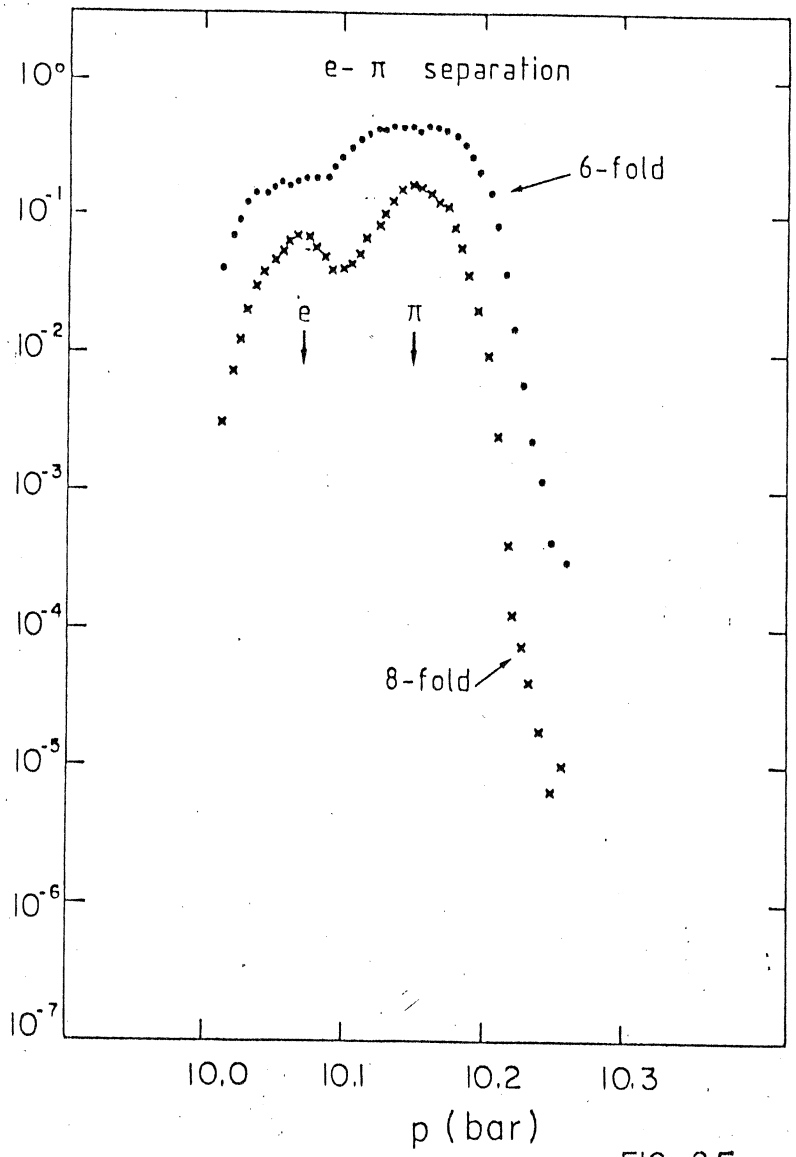
e- π separation
6-fold
8-fold
e
π
10°
10⁻¹
10⁻²
10⁻³
10⁻⁴
10⁻⁵
10⁻⁶
10⁻⁷
10.0
10.1
10.2
10.3
p (bar)

FIG. 25

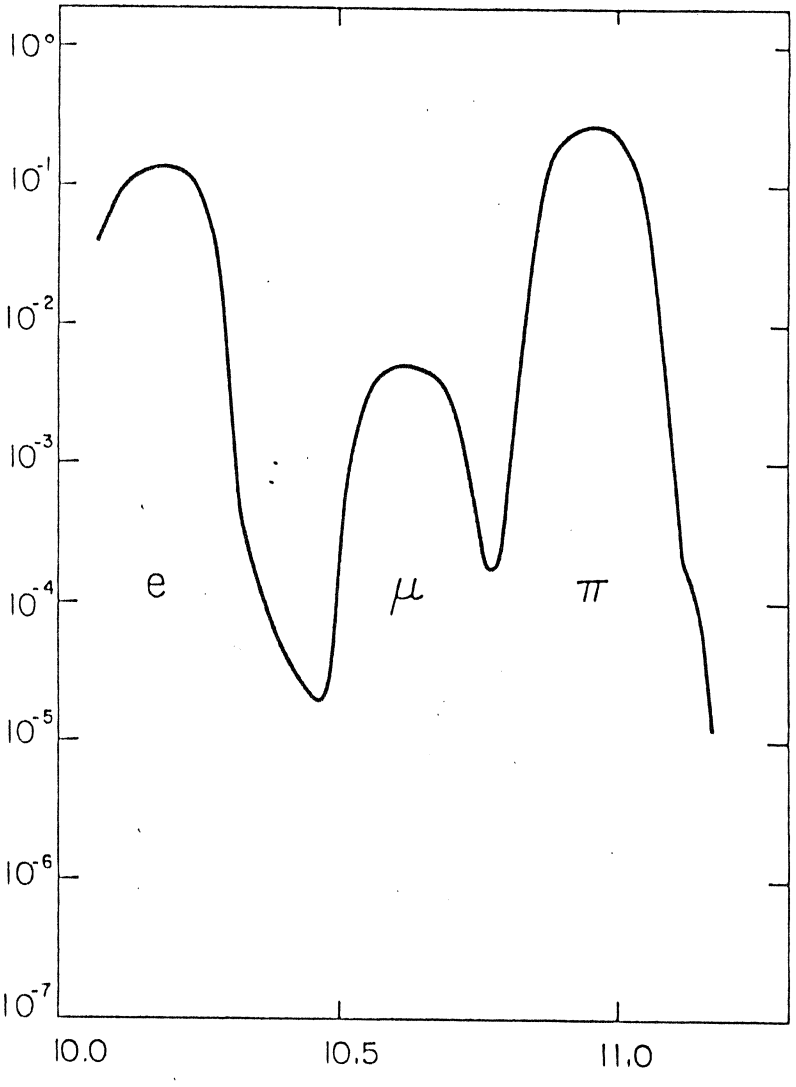
e
μ
π
10°
10⁻¹
10⁻²
10⁻³
10⁻⁴
10⁻⁵
10⁻⁶
10⁻⁷
10.0
10.5
11.0
p (bar)

FIG. 26